공학석사학위논문

Development of Tidal Energy Extraction Model for the Transverse Horizontal Axis Water Turbine Considering Flow Velocity Profile

유속 분포를 고려한 Transverse Horizontal Axis Water Turbine 의 조류 에너지 추출 모델 개발

2019 년 8 월

서울대학교 대학원

건설환경공학부

이창희

Abstract

Development of Tidal Energy Extraction Model for the Transverse Horizontal Axis Water Turbine Considering Flow Velocity Profile

Lee, Chang Hee

Department of Civil and Environmental Engineering

Graduate School of Seoul National University

The evaluation of efficiency is important in assessing the economical and engineering feasibility for the deployment of the tidal energy turbines. Since the efficiency is determined by the various factors such as the velocity, density of fluid, and material and geometric properties of turbine, simplified approach need to be introduced for reducing the complexity of those factors. As an example of simplified models, the linear momentum actuator disc theory (LMADT) has been widely adopted to analyze the performance of the axial-flow turbine in a uniform flow since this method provides a set of the analytic solutions by simplify turbine

as a disc which is the source of constant thrust acting in the opposite direction to the flow.

Among many tidal devices, Oxford university recently introduced the Transverse Horizontal Axis Water Turbine (THAWT), which is a type of the cross-flow turbines suggested by McAdam (2011). THAWT has several advantages. It has a constant efficiency in both flow directions and can be easily extended laterally, and is structurally stable. However, it is not possible to apply LMADT directly to the analysis of THAWT due to the more complex mechanism than the axial-flow turbine. Also, for cross-flow turbine, the presence of the flow velocity distribution affects the power coefficient of a turbine since the blade of a turbine rotates reversely of flow direction during half of a cycle.

In this research, the power coefficient of THAWT with the velocity profiles is obtained by the blade element momentum theory (BEMT), which analytically assesses the physical properties acting on the blades differently from the typical LMADT. It has two advantages in analyzing the cross-flow turbine. One is that it overcomes the limitation of LMADT, and another is that it can consider the velocity by determining the total force acting on the blade directly with the lift and drag forces. Constructing a set of simple analytic model based on BEMT, the power coefficient of turbine will be found numerically. After all, the velocity induction factor which is adopted from the LMADT and the friction factor considering the normal force and frictional factors are selected as the adjustment parameters to

validate by comparing the results from the small-scale turbine model made from 3D printer.

Based on the constructed numerical model and experimental results, the factors which affect the tip speed ratio of turbine are expressed as the combination of the non-dimensional parameters made by the water depth, turbine diameter and upstream time mean velocity of flow. The adjustment parameters (velocity induction and friction factor) can be rearranged into the empirical relation, it shows the $R^2 = 0.8340$. From this study, it can provide the simple and fast results to evaluate the energy potential of certain estuarine area where the water depth and velocity profile is specified.

Keywords: Tidal energy, THAWT, BEMT, Cross-flow turbine

Student Number: 2017-29440

Table of contents

Nomenclature

a	velocity induction factor	
A	area of the turbine	$[\mathrm{m}^2]$
A_t	frontal area of the turbine	$[\mathrm{m}^2]$
B	blockage ratio	
c	chord length of blade	$[\mathrm{m}]$
c_d	chord to diameter ratio	
C_D	drag coefficient	
C_L	lift coefficient	
C_P	power coefficient	
C_T	coefficient of thrust	
d	turbine diameter	$[\mathrm{m}]$
D	drag force	[N]
E	extracted energy by turbine	[J]
F	force	[N]
F_N	normal force	[N]
F_T	tangential force	[N]
$\mathrm{Fr} = \frac{u}{\sqrt{gh}}$	Froude number	
g	gravitational acceleration	$[\mathrm{m/s}^2]$
h	depth of flow	$[\mathrm{m}]$

L	lateral length of turbine array	$[\mathrm{m}]$
L	lift force	$[\mathrm{N}]$
L_d	relative lateral length	
m	mass per unit length	$[\mathrm{kg/m}]$
N	number of actuator disc in tandem	
p	pressure	$[\mathrm{N/m^2}]$
P	power	$[\mathrm{W}]$
q	flow rate	$[\mathrm{m^3/s}]$
r	radius of blade	$[\mathrm{m}]$
$\mathrm{Re} = \frac{uL}{\nu}$	Reynolds number	
T	thrust	$[\mathrm{N}]$
u	flow velocity	$[\mathrm{m/s}]$
V_G	relative velocity gradient	
V_R	relative velocity between blade and flow	
α	angle of attack	$[\mathrm{rad}]$
α_2	velocity induction factor	
η	efficiency	
θ	location of each blade	$[\mathrm{rad}]$
λ	tip speed ratio	
ν	kinematic viscosity	$[\mathrm{m^2/s}]$
ρ	density of fluid	$[\mathrm{kg/m^3}]$
ρ_b	density of blade material	$[\mathrm{kg/m^3}]$
ω	angular velocity of turbine	$[1/\mathrm{s}]$

Subscripts

b	blade
m	model
p	prototype
t	turbine
i	index number of blade

List of figures

List of tables

1. Introduction

1.1. Research Background

Tidal power has been developed for a long time and became one of technologies, which are considered as a technically and economically feasible resource now (McAdam, 2011). The advantage of tidal power is in that forecast is very reliable over the long period (Denny, 2009). Thanks to its consistency, it will be less challenging source of electricity than other forms of unpredictable renewable energy. However, among the numerous models for the analysis of turbine devices, there is no best design criteria except wind power generations (Khan *et al*., 2009).

For the economical and engineering feasibilities of renewable energy, the efficiency of turbine is commonly used for analysis in industry. Instead of direct displaying the output of electricity, people have used the power coefficient of turbine which is defined as the ratio of the power generated by the turbine to the kinetic energy of fluid. To obtain this, the linear momentum actuator disc theory (LMADT) has been adopted to analyze the axial-flow turbine (Draper, 2011). While the various factors such as the velocity, density of fluid, and material and geometric properties of turbine affect the power coefficients, LMADT can give a solution of the power coefficient and the other properties of flow in upstream and downstream. LMADT is in an analytic form by assuming the turbine simply as a

single disc, which is a source of constant thrust acting on the flows in the opposite direction (Houslby et al, 2008).

Two types of turbine are widely used in renewable energy industry; axial-flow turbine and cross-flow turbine (O'Rourke et al., 2010). The axial-flow turbine is the turbine that its rotation axis is parallel to the flow direction, while the rotation axis of the cross-flow turbine is perpendicular to the flow direction. The axial-flow turbine has more potential (to generate energy than cross-flow turbine in an equally given flow condition (Carrigan et al., 2012). However, it is unidirectional turbine and to designed to generate full electric energy when it is deployed in a one-directional flow. Since the cross-flow turbine is designed for the multidirectional flows, it has relatively low efficiency in a unidirectional flow but is more proper in tidal flow which has bi- or more directional flow directions.

Among the various kinds of turbines, the technical feasibility of the transverse horizontal axis water turbine (THAWT) was discussed by McAdam (2011) in Oxford University. Although its axis is in horizontal, it has the common properties of typical cross-flow turbine since the fluid flows the turbine perpendicular to its axis. This recently invented device shows technically and economically feasible results both in numerical and experimental studies. Also, this device has great expandability because of its stable structure (McAdam, 2011).

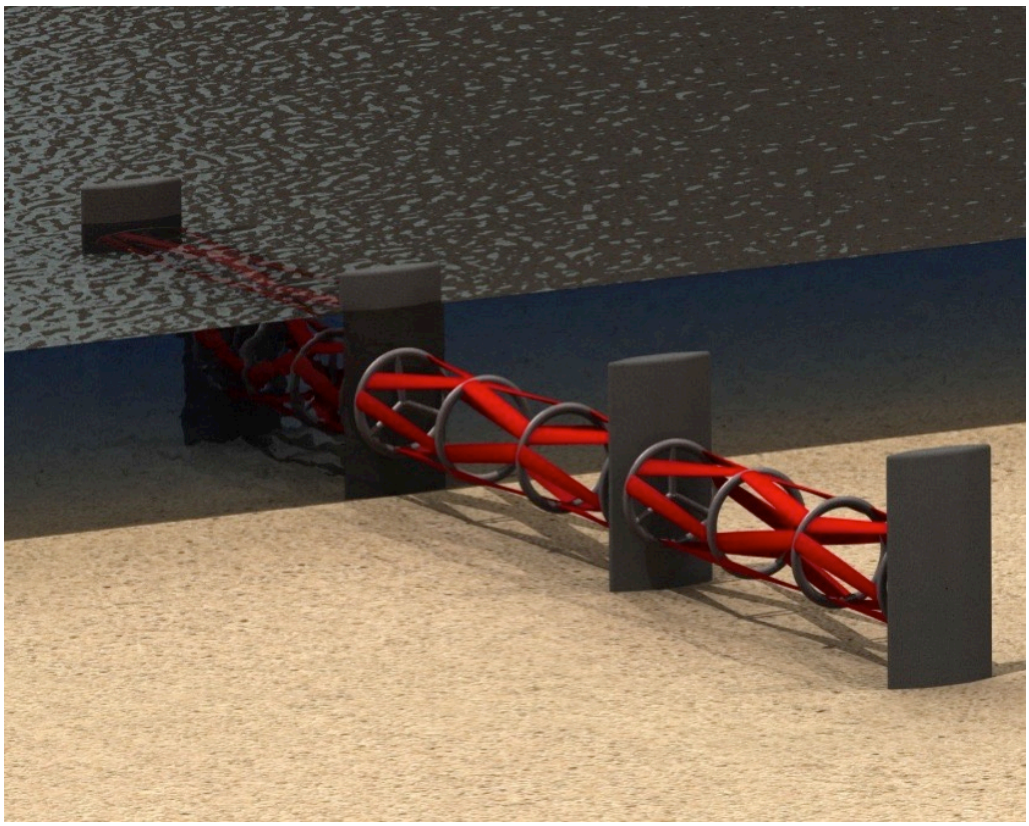

Fig. 1. Rendered CAD image of the THAWT device with the sea cut away (adopted from McAdam, 2011)

Through the history, however, the prediction of extracted energy for cross-flow turbine is more difficult issues than axial-flow turbine because of the wake effect between the turbine blades (Maître, 2013). Cleary, it is difficult to apply the LMADT directly to other types of turbines except axial-flow turbines, and it is also hard to consider the flow velocity distribution because it assumes the uniform flow (Paraschivoiu, 2002). Despite of the difficulty for cross-flow turbine with its energy assessment, to make the economically meaningful tidal farms, it is

important to make simple analysis model to evaluate the potential of target site with a few variables such as fluid velocity, turbine size, location depth of the turbine, etc.

In previous research for THAWT by McAdam (2011), it does not consider the effect of the velocity profile. For cross-flow turbine, the presence of the flow velocity distribution will affect the power coefficient of turbine since the blade rotates reversely to the flow direction during half of a cycle. Therefore, this research will obtain the power coefficient of THAWT in non-uniform by applying the blade element momentum theory, which can assess the physical properties acting on the blades instead of typical LMADT. It has two advantages to analyze the cross-flow turbine. One is that it overcomes the limitation of LMADT, and another is that it can consider the velocity profile since the blade element method considers the force acting on the blade directly by lift and drag force. After constructing a simple analytic, the power coefficient of turbine in equilibrium state will be found numerically and validated with the experimental data. The results determine whether the mean velocity and velocity profile are appropriate to install the tidal turbine.

1.2. Research Objectives

The two main objectives in this research are suggested below.

First, the present work proposes an analytical model to describe the motion, force, and energy for the Transverse Horizontal Axis Water Turbine considering the properties of the flow and turbine. So far, there were not a simple model constructed for THAWT device in two reasons. One is that THAWT is recently invented and another is that there are not popular to use simplistic model for the cross-flow turbine. The following variables will be important in constructing the model. For the flow, the mean velocity, and the flow velocity profile are main factors among the various input variables. For the turbine, the size and the material type could be deterministic parameters. Therefore, the derived model can calculate the angular velocity, power, and energy, which are generated at each time step and applicable to the tidal farm construction in estuarine area.

Second, the constructed model is validated by the comparison with the experimental results. It is important to validate the constructed model since the model has no analytical exact solution. Based on dimensional analysis, the geometric, kinematic, and dynamic similarities should be guaranteed for the experimental work. Flow properties in the experiment will be determined by the Vectrino, which is a velocimetry based on the acoustic Doppler effect of sounds in the water. Since the model equation requires the flow velocity profile at the

position of installed device, the velocity profile should be determined in experiment. Also, the angular velocity and the force acting on the turbine blade will be determined from image processing. Among the various variables of turbine, the angular velocity is most important factor of analyzing turbine device since it determines the generated energy by itself. With this information, the simplified model will be validated and calibrated to match with the real condition obtained from experiment.

1.3. Outline

In chapter 2, the previous researches are reviewed mainly focusing on the theoretical base and types of turbine. Among the several types of turbine, the analysis of the axial-flow turbine and the cross-flow turbine will be discussed to apply and construct simplified model.

In chapter 3, firstly, the dimensional analysis is performed to capture the important non-dimensional parameters representing force balances of turbine device. And then, a simplified model of the cross-flow turbine to analyze the turbine will be constructed with the Blade Element Momentum Theory (BEMT) similarly to the Linear Momentum Actuator Disc Theory (LMADT) concept.

In chapter 4, experimental setups are determined by satisfying the similarity criteria. The chapter describes the ways of measuring velocity profile of flume, making turbine device, and simple image processing technique to capture the angular velocity of module. The flow properties will be measured by the Vectrnio. Also, the method of image process which was used in measuring the angular velocity will be explained in detail.

In chapter 5, results from experimental work will be used to calibrate and validate the model results. Two parameters named velocity induction factor and friction coefficient will be used to calibrate the model. Based on the Froude number and blockage ratio, the two coefficients are matched to empirical formula.

2. Background theories

The classification of turbine, and methods for analyzing turbine will be provided in this section. Although wind and tidal turbines share the principals of which the fluid particles hit the blade and transfer the kinetic and potential energy, the operating condition for them can be quite different each other. Please note that Linear Momentum Actuator Dis Theory (LMADT) states for steady and analytic approaches by assuming turbine as a disc for constant source of thrust (Batten *et al*., 2013). On the other hand, blade element momentum theory is only applicable only if the experimental data of lift and drag coefficient is given for the target blade shape (Anderson, 2010).

2.1. Types of turbine device

The major tidal devices can be categorized into 3 types; Axial-flow turbine, Cross-flow turbine, Oscillating and other types of device. While the THAWT is classified as a cross-flow turbine, the axial-flow turbine is most popular and widely used for tidal power generation (Khan *et al*., 2009). Also, the axial-flow turbine has more theoretical models to describe it than the cross-flow type one. Such theories can give the insight of the discussion since the principal of energy extraction is almost same.

2.1.1. Axial-flow turbine

Axial-flow turbine is most popular and common both for wind and tidal energy generation (Khan *et al*., 2009). The axial-flow turbine is defined as the turbine that its axis is parallel to the direction of flow. In Fig.2., the typical shape of axial-flow turbine is suggested. Since it has a large amount of previous research by the wind energy industry in terms of its dynamic properties and structural aspects in design, it is believed to have a high confidence in the technology. It has advantage of accurate prediction of the performance using various techniques (Batten *el al.*, 2006). Also, among many turbine devices, the axial-flow turbine has relatively efficient. However, it has limit since its diameter (or size) cannot be increased significantly because of the presence of flow depth unlike the wind condition (Bryden *et al.*, 1998). Also, it is hard to apply to the bidirectional flow. Among various kinds of applications, the basis of them is the Linear Momentum Actuator Disc Theory (LMADT) which is proposed by Froude (1889), further advanced by Betz (1920), and recently extended to the open channel flow by Houlsby et al (2008). These theories are discussed in chapter 2.2 in detail.

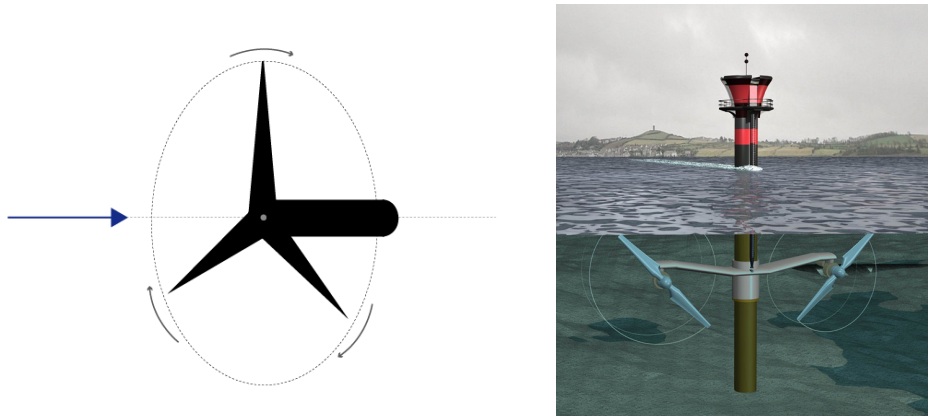

Fig. 2. Schematic figure of axial-flow turbine (left), marine current power* (right)

Source: * www.memim.com

2.1.2. Cross-flow turbine

The concept of cross-flow turbine devices is originally from Darrieus turbine which is patented by the French aeronautical engineer Georges Jean Marie Darrieus (Darrieus, 1931).

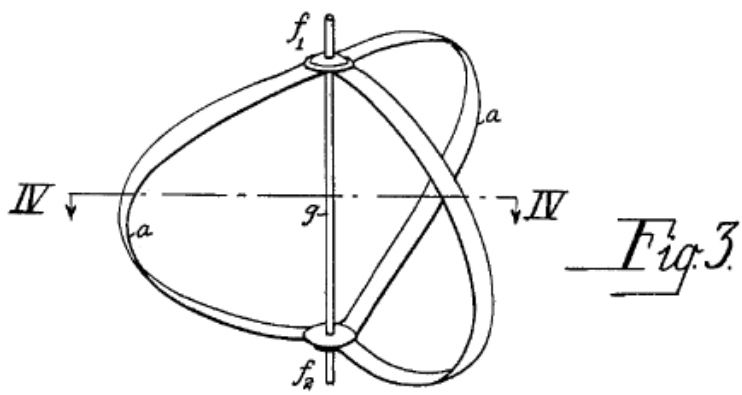

Fig. 3. Darrieus turbine patented by Georges Jean Marie Darrieus (Darrieus, 1931)

In Fig. 4., the schematic figure of cross-flow turbine shows that the rotational axis is perpendicular to the flow direction unlike axial-flow turbine. Although this concept of vertical axis turbine is not very popular in the wind industry in the presence of the efficient axial-flow turbine, the cross-flow concept has been adopted for some kinds of tidal devices (O'Rourke et al., 2010). It has strong advantage its consistency for any direction of flow and less effort to control yaw mechanisms rather than axial-flow device (Fujisawa & Shibuya, 2001).

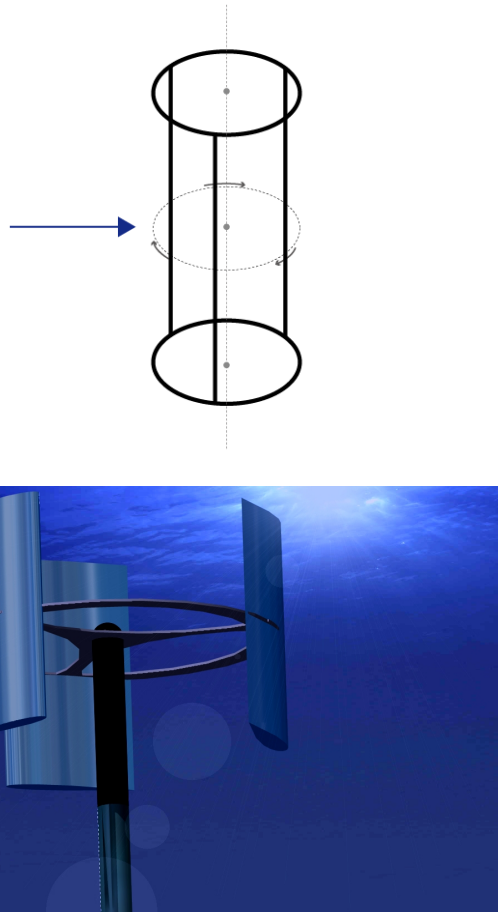

Fig. 4. Schematic figure of cross-flow turbine (left), vertical-axis tidal turbine* (right)

Source: * www.esru.strath.ac.uk

The cross-flow turbine has advantages for the consistency while it is applied in tide since it easily deals with bidirectional flow. However, it is less efficient than axial-flow turbine. The analysis of cross-flow turbine can be categorized into the momentum model which has analytic form, the vortex model, and the CFD based model (Maître *et al.,* 2013). In this thesis, the approaches of momentum based

model is discussed. Starting from Templin (1974), namely the single streamtube model, the analytic derivations are followed for the multiple streamtubes model (Strickland, 1975), the double-multiple streamtubes model (Loth & McCoy, 1983, Paraschivoiu & Delcalux, 1983). The blade characteristics are used for calculating momentum based on lift and drag forces in above researches.

2.2. Models for axial-flow turbine

2.2.1. Linear Momentum Actuator Disc Theory (LMADT)

The Linear Momentum Actuator Disc Theory (LMADT) is an analytic approach that presents solution for the physical properties of an axial-flow turbine in incompressible and viscous fluid can attain through mass conservation, momentum conservation and energy conservation equations. The energy production through the turbine is always smaller than the result of LMADT assuming inviscid flow due to energy loss by viscosity and friction of the turbine rotors. The derivation process in this section is following up the steps from Houlsby *et al* (2008).

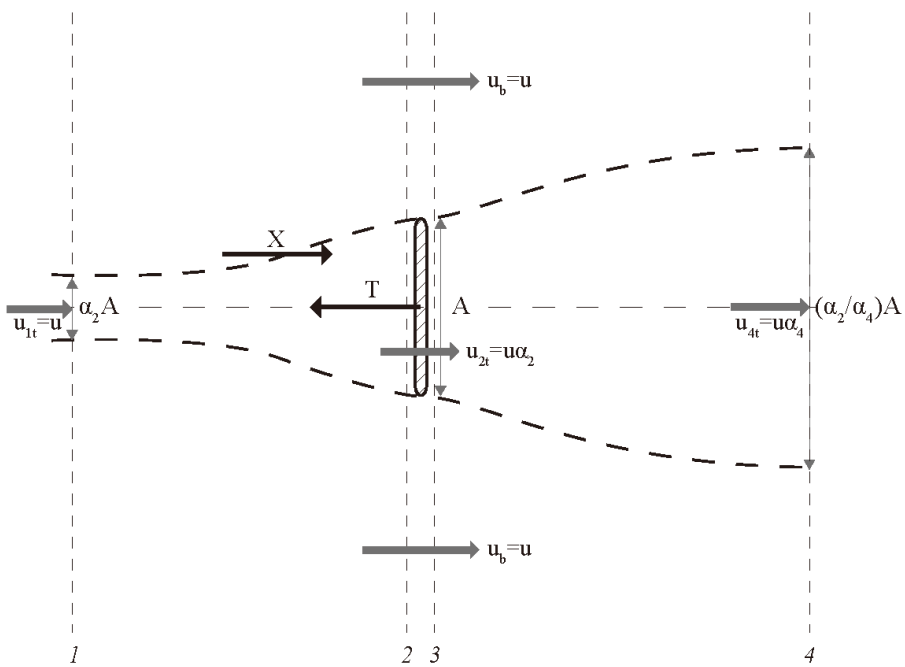

Fig. 5. Geometry of LMADT in infinite flow (Houlsby *et al.*, 2008)

The standard LMADT was introduced by Froude (1889) and further advanced by Betz (1920). In Fig. 5, the turbine is converted to the disc and the given area is divided into the turbine area and by-pass area. Along the flow, two areas are separated by the control volume. After that, the 4 sections are appeared across the flow. First, the section 1 means far upstream from the turbine. Therefore, the velocity and pressure are constant. Second, the section 2 in figure 6 means very close area from the turbine which has direction headed for upstream. Third, the section 3 also means very close area from the turbine which has direction headed for downstream. Finally, the section 4 means far downstream from the turbine which has uniform pressure and velocity.

For the convenience of the expression, the criterion of the velocity is section 1, u, and the area is section 2 (size of the turbine), A. Each part of the section, the value of properties such as pressure, velocity can be divided into subscript. For example, *P* means the pressure and numbers in the subscript means the section, and b of subscript means by-pass, t means turbine area, etc. P_{2b} means the pressure of section 2 in by-pass area, and u_{4t} means the velocity of section 4 in turbine area. The other main coefficient is α_2, α_4 which is the velocity coefficient of section 2 and 4 respectively. $u_2 = u\alpha_2$, $u_4 = u\alpha_4$. From these coefficients, the other properties like area can be expressed as convenient way.

The following assumptions are suggested for the derivation. First, the velocity and pressure is constant at section 1. Furthermore, the velocity has been reduced at Section 2, and further reduced at section 4. Through the area, by the interference of turbine, the velocity should be decreased. Finally, pressure is uniform across the flow at section 4.

Between the section 1 and 2, which are in the same control space, we can apply the Bernoulli Equation. For the fluid which has the density ρ, the result is

$$p + \frac{1}{2}\rho u^2 = p_{2t} + \frac{1}{2}\rho u^2 {\alpha_2}^2. \tag{2.1}$$

Also, between the section 3 and 4, which are in the same control volume, we can apply the Bernoulli Equation. The result is

$$p_{3t} + \frac{1}{2}\rho u^2 {\alpha_2}^2 = p_{3t} + \frac{1}{2}\rho u^2 {\alpha_4}^2. \tag{2.2}$$

The net force in turbine should be in equilibrium condition. The only force about making thrust is the pressure difference between section 2 and 3. Following equation shows that.

$$p_{2t} - p_{3t} = \frac{T}{A} \tag{2.3}$$

where T is the thrust of a disc.

From the above 3 kinds of equation ((1), (2), (3)), we can find the relationship about the trust and the velocity of the fluid.

$$\frac{1}{2}\rho u^2(1-\alpha_4{}^2)=\frac{T}{A} \tag{2.4}$$

In the turbine section, we can apply the Momentum Equation. For the net change of momentum in by-pass flow X , it follows

$$X-T=\rho q_t(u_{4t}-u_{1t})=\rho u^2 A\alpha_2(\alpha_4-1). \tag{2.5}$$

There is no net change of momentum in by-pass flow (there is no velocity change in by-pass area), so $X=0$.

$$\frac{T}{A}=\rho u^2\alpha_2(1-\alpha_4) \tag{2.6}$$

From the equation (4), (6) we can find the relationship between the two coefficient about velocity.

$$\alpha_2=\frac{1+\alpha_4}{2} \tag{2.7}$$

To find the power absorbed by the turbine, we should use the equation (2.4) and (2.7). The power absorbed by the turbine can be calculated by multiplying thrust and velocity in section 2.

$$P=T\alpha_2 u=\frac{1}{2}\rho u^3 A\frac{1+\alpha_4}{2}(1-\alpha_4)^2=\frac{1}{2}\rho u^3 AC_P \tag{2.8}$$

The maximum power is extracted when the power coefficient C_P is maximized as a function of α_4. We can use calculus to find the optimum condition of the coefficient.

$$\frac{dC_P}{d\alpha_4}=0$$

For $0 < \alpha_4 < 1$, the maximum value of C_P is 16/27 at $\alpha_4 = 1/3$. Also, $\alpha_2 = 2/3$.

From Equation 4, we can set a dimensionless term of thrust coefficient.

$$T = \frac{1}{2}\rho u^2 A(1-\alpha_4{}^2) = \frac{1}{2}\rho u^2 A C_T \tag{2.9}$$

At $\alpha_4 = 1/3$ and $C_T = 8/9$.

To express the thrust in terms of local velocity, equation 9 can be modified.

$$T = \frac{1}{2}\rho u_2{}^2 A C_{TL} = \frac{1}{2}\rho u^2 A \alpha_2{}^2 C_{TL} \tag{2.10}$$

From Equation 9, 10 $C_{TL} = C_T / \alpha_2{}^2$ and at optimum condition $C_{TL} = 2$.

The limitation of this derivation is that we assumed only axial components of velocity (ignore the radial and tangential velocities). In addition, ambiguity of the pressure along the boundary lines means unknown force *X* cannot be derived from the pressure. Finally, far downstream from the turbine (Section 4), by the wake mixing process there is an additional energy loss.

2.2.2. LMADT in open channel flow

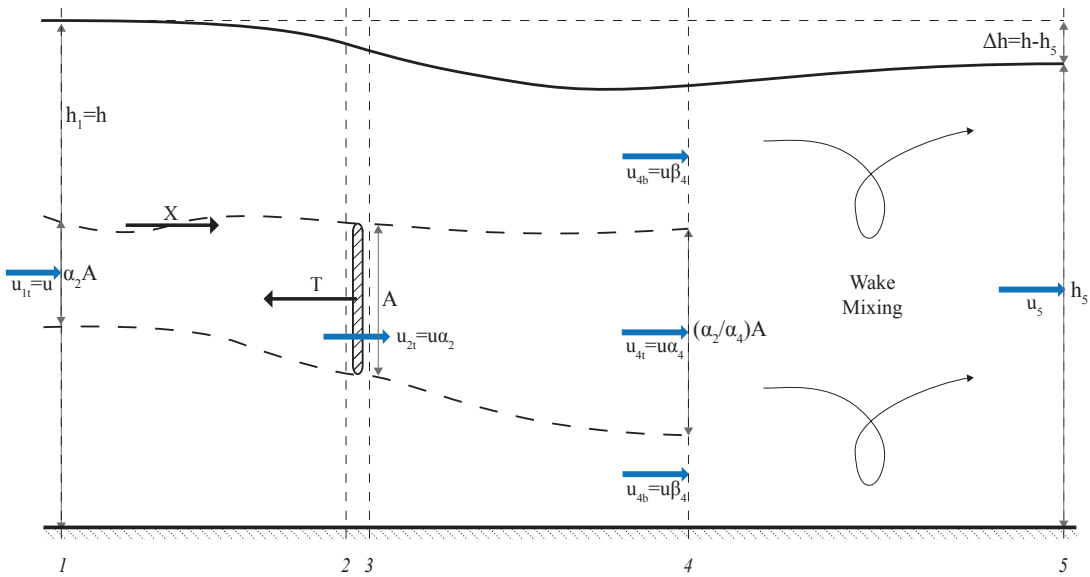

Fig. 6. Geometry of LMADT in an open channel flow (Houlsby *et al.*, 2008)

Unlike classical LMADT, which was applied to early wind turbines, Houlsby *et al* (2008) extended the LMADT to open-channel condition to accommodate free surface and vertical pressure changes for tidal power generation applications. When there is an axial turbine under numbered conditions, the flow of fluid from upstream 1 decelerates as it passes past turbines 2 and 3, and is divided into two regions 4 to form a uniform flow 5.

The LMADT in the open channel can be characterized by several dimensionless numbers. First, the Froude number is defined by the upstream flow velocity u_2, gravity acceleration g and upstream water depth h as follows

$$Fr = \frac{u}{\sqrt{gh}} \tag{2.11}$$

Next, the blockage ratio of the turbine in the channel is defined as *B* and defined as follows. Here, A_t is the width of the turbine, and A_c is the width of the zone.

$$B = \frac{A_t}{A_c} \tag{2.12}$$

The induction factor, which is the rate at which the flow velocity is decelerated in the turbine, is as follows. Here u_t is the flow rate through the turbine zone.

$$\alpha_2 = \frac{u_t}{u} \tag{2.13}$$

The coefficient of thrust C_T is defined as the value of the thrust generated by the turbine by the product of the dynamic pressure at the upstream and the area. Here, T means the thrust produced by the turbine, and ρ means the density of the fluid.

$$C_T = \frac{T}{\frac{1}{2}\rho u^2 A_t} \tag{2.14}$$

The above-mentioned dimensionless numbers have the following relationship when the change of the downstream water depth for the upstream water depth is taken as Δh.

$$\frac{1}{2}\left(\frac{\Delta h}{h}\right)^3-\frac{3}{2}\left(\frac{\Delta h}{h}\right)^2+\left(Fr^2\left(\frac{BC_T}{2}-1\right)+1\right)\left(\frac{\Delta h}{h}\right)-\frac{BC_T}{2}Fr^2=0 \tag{2.15}$$

The kinetic power coefficient of the turbine (C_{pk}) can be simply calculated as follows.

$$C_{pk}=\alpha_2 C_T \tag{2.16}$$

Since the system is a completely invisible fluid flow, there is a unique energy loss in the mixing process after the turbine has passed. Therefore, the efficiency of the above system (η) can be regarded as a value considering the energy extracted from the turbine and the energy loss caused by the mixing of the wake due to the turbine. Therefore, the following relationship is derived.

$$\eta=\frac{C_{pk}}{C_{pk}+C_{pk-mixing}} \tag{2.17}$$

The energy loss occurs through mixing by the wake of the turbine and the flow rate difference of the surrounding flow. Under a given water depth change condition, the energy loss due to mixing can be reduced by increasing the blockage ratio or by reducing the difference in flow rate between the wake and the surrounding flow so that the flow after the turbine is uniform.

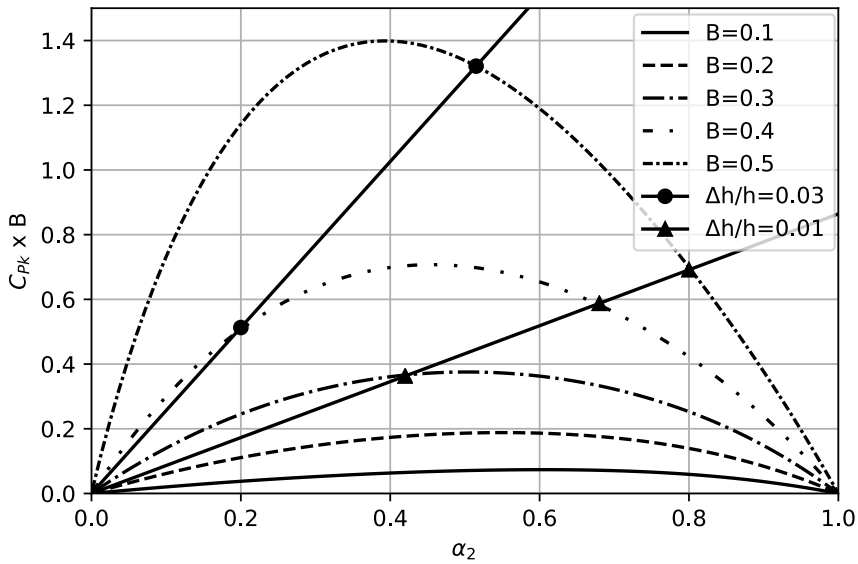

Fig. 7. Kinetic power coefficient multiplied by blockage ratio at Fr = 0.15 for velocity induction factor (McAdam, 2011)

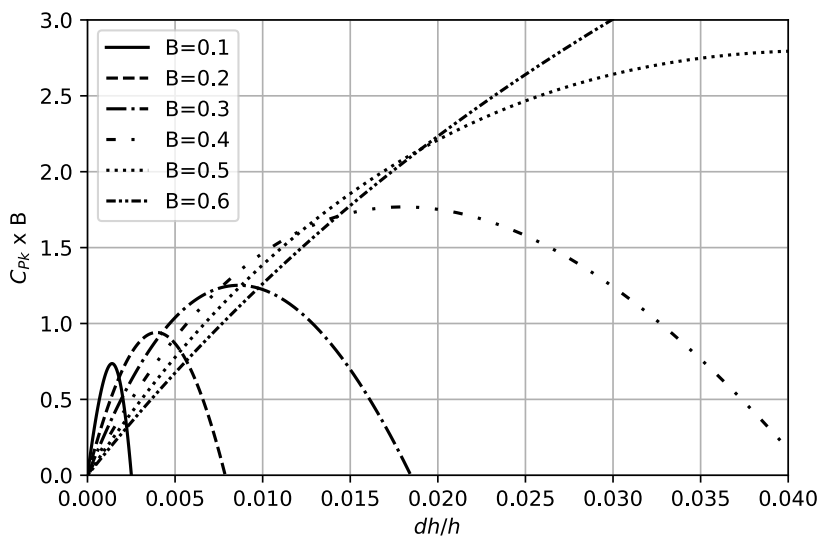

Fig. 8. Kinetic power coefficient multiplied by blockage ratio at Fr = 0.15 for depth change ratio (McAdam, 2011)

The Fig. 7 and 8 shows the turbine production energy according to several blockage ratios under fixed water depth changing conditions of Froude number (Fr=0.15). It can be seen that the larger the area occupied by the turbine under the fixed depth variation, the greater the energy production. However, the size of the turbine on the coast is constrained by environmental, social, or other factors. On the other hand, if you use a small turbine, you will not get enough energy efficiency with a single turbine and you will have to deploy a larger number of turbines to reach your target energy output. It shows the energy that can be produced when the water depth change of 3% occurs. As the blockage ratio increases, the energy production increases dramatically. However, under the relatively low water depth change (1%) condition, the increase of the blockage ratio is not as effective as in 3 % depth change.

2.3. Models for cross-flow turbine

2.3.1. Blade Element Momentum Theory (BEMT)

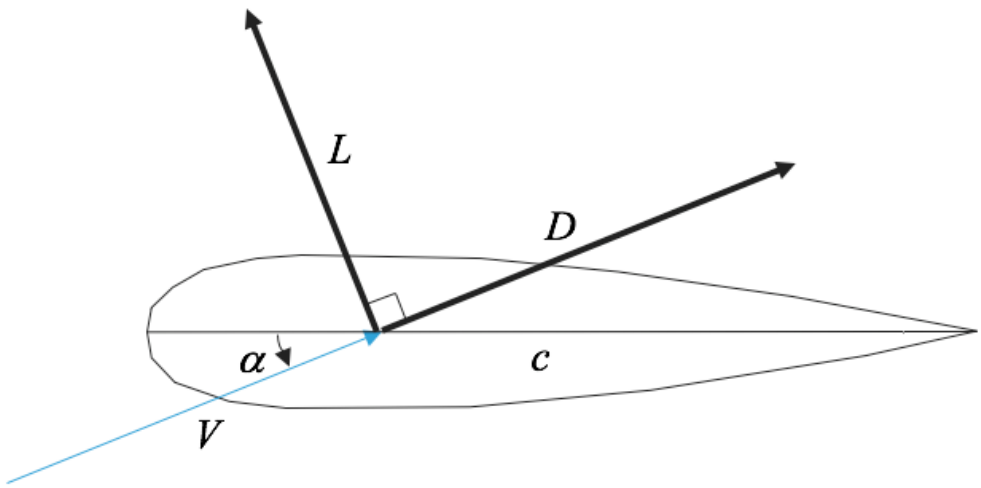

Fig. 9. Force diagram acting on the typical airfoil (NACA 0018) (Anderson, 2010)

Fig. 9 shows a typical airfoil used for turbine devices. To consider the forces acting on the blade directly, the BEMT is used for modeling vertical axis turbine devices in this research. The BEMT is a theory which is widely used in aerodynamics to interpret flow around blades used for airfoils. When the object is in a flow, two types of forces are acting on the object; one is the drag force and another is the lift force. The former is the force which is parallel to the flow and the latter is normal to the flow. It defines the forces in airfoil (or hydrofoil) using geometric property of blade (chord length) and fluid velocity. The equations of the lift L and the drag D are given below.

$$L = \frac{1}{2}\rho V^2 c C_L \tag{2.18}$$

$$D = \frac{1}{2}\rho V^2 c C_D \tag{2.19}$$

where ρ is the density of fluid, V is the fluid velocity, c is the chord length of airfoil, α is the angle of attack, C_L is the lift coefficient and C_D is the drag coefficient.

The important thing is to determine C_L and C_D which are influenced by the shape of blade, the angle of attack and the Reynolds number. There are various blade shapes and so the corresponding lift and drag coefficients. The present work uses the experimental results of Sheldahl & Klimas (1981) for numerical analysis of vertical axis turbine.

The value between the discretized experiment results will be interpolated by cubic spline interpolation with free end condition. Since this airfoil has symmetrical shape, the values can cover the whole ranges for angle of attack ($0 \le \alpha \le 2\pi$).

The Fig. 10, 11, 12 and 13 give the aerodynamic coefficient of NACA 0018 airfoil from the experimental data (Sheldahl & Klimas, 1981). Fig. 12 and 13 stand for the lift coefficients and it is noted that Reynolds number and angle of attack strongly affect the lift coefficients. However, if the angle of attack is larger than $30°$, only the angle of attack determines the lift coefficient of airfoil. Likewise, as shown in Fig. 12 and 13, the drag coefficient is also determined by the Reynolds number and the angle of attack until α is under $20°$. By Using this experimental data and properties, the lift and drag coefficients can be determined for the most cases except of the case that Reynolds number is larger than 5.0×10^{6}. For other Reynolds number, the interpolation is applied between the nearest values of experimental results. For $\nu = 10^{-6}\,\mathrm{m}^2/\mathrm{s}$, it happens that the product of velocity and characteristic length is larger than $5\mathrm{m}^2/\mathrm{s}$. For example, the calculation of $1\mathrm{m}$ chord of blade has risk if the flow whose velocity is larger than $5\mathrm{m/s}$.

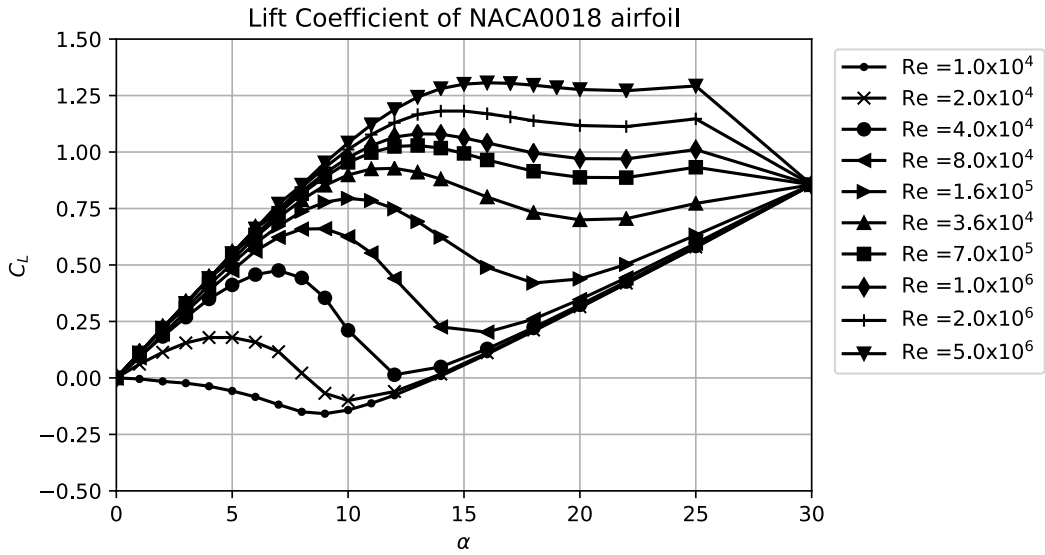

Fig. 10. Lift coefficient of NACA 0018 airfoil, $0° \le \alpha \le 30°$ (Sheldahl & Klimas, 1981)

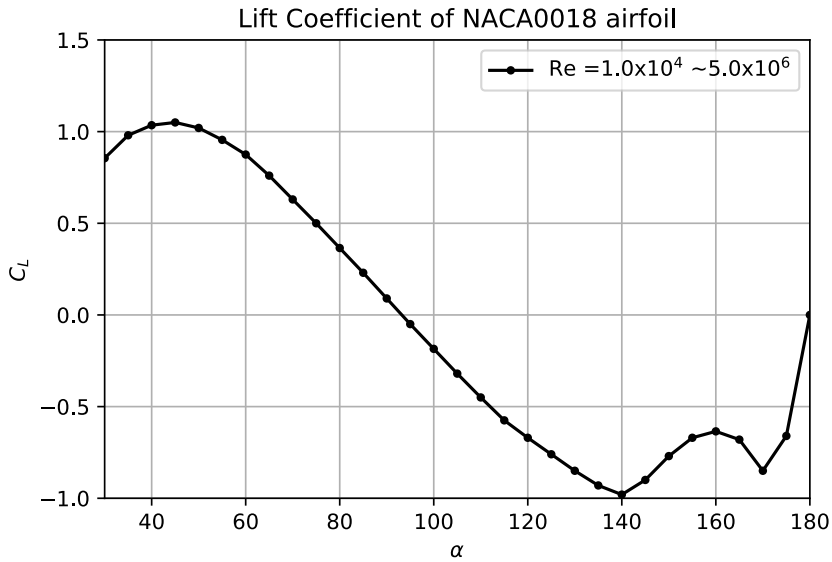

Fig. 11. Lift coefficient of NACA 0018 airfoil, $30° \le \alpha \le 180°$ (Sheldahl & Klimas, 1981)

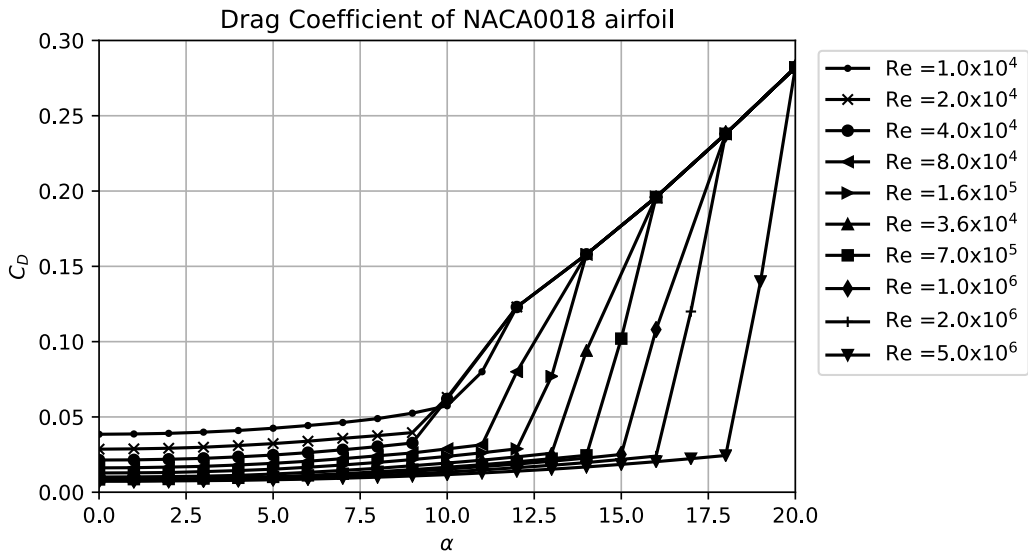

Fig. 12. Drag coefficient of NACA 0018 airfoil, $0° \le \alpha \le 20°$ (Sheldahl & Klimas, 1981)

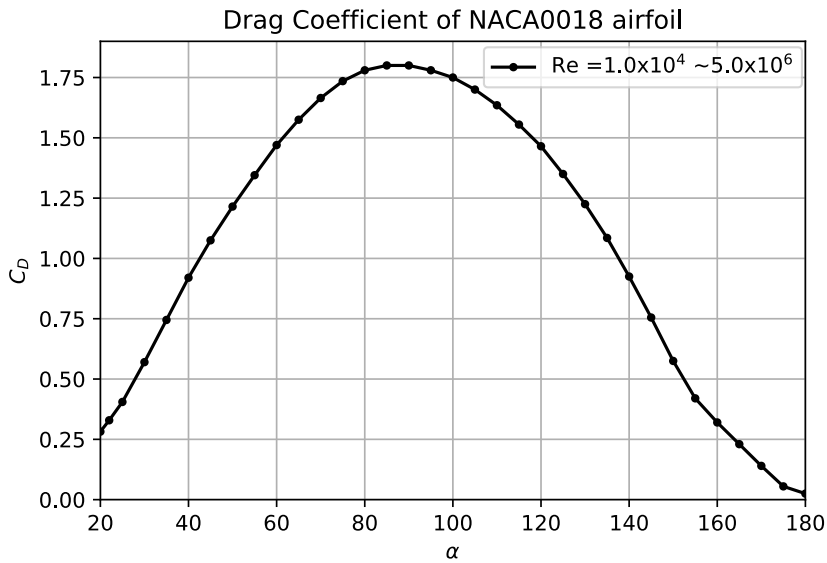

Fig. 13. Drag coefficient of NACA 0018 airfoil, $20° \le \alpha \le 180°$ (Sheldahl & Klimas, 1981)

2.3.2. LMADT for cross-flow turbine

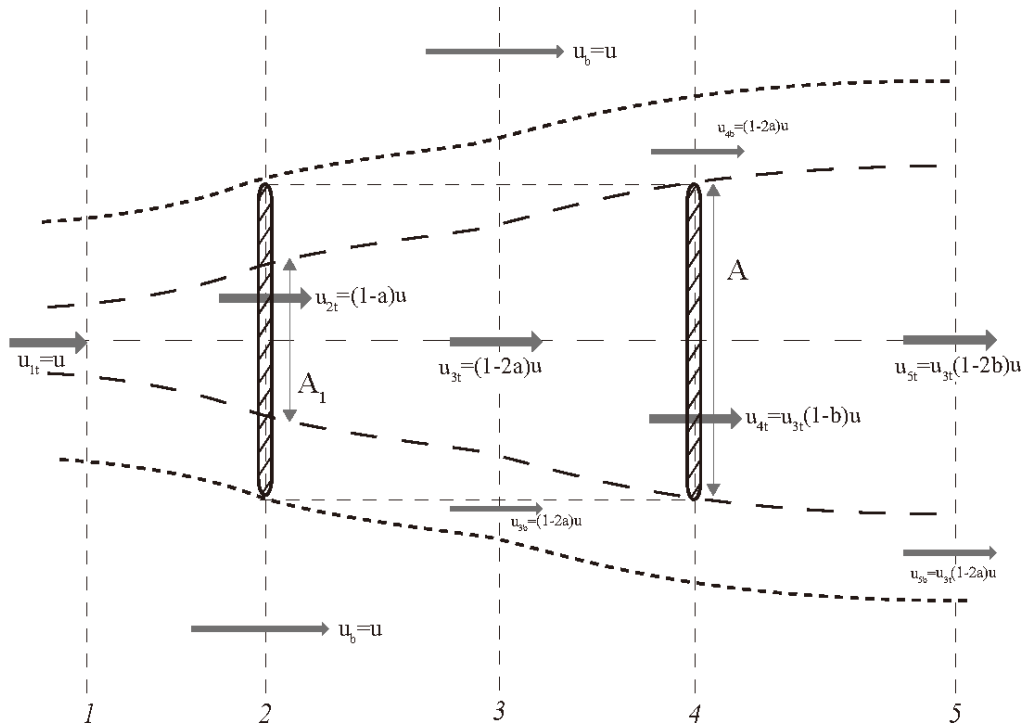

Fig. 14. Geometry of two actuator discs in series (Newman, 1984)

The torque in single actuator disc gets great value in case of the location of the blades locating at upstream and downstream of its axis. Where two turbines are deployed along the flow axis, torque in a actuator disc has maximum. So the double actuator disc model can be more effective method to represent the model. Then, the maximum $C_P = 16/27$ calculated at section 2.1 should be reconsidered in this section.

The two actuator discs are arrayed in tandem, and the area of each disc is A. A_1 is the area of the upstream part of disc included in the same control space as the downstream part of disc. The space between the two discs is vented and the pressure there has same value as the pressure far upstream of the total flow.

The only thing to be done is dividing the sections and employing a new coefficient b, which is an interference coefficient of the second discs.

The power coefficients of each disc are

$$C_{P1} = 4(a^3 - 2a^2 + a) \tag{2.20}$$

$$C_{P2} = 4(1-2a)^3(b^3 - 2b^2 + b). \tag{2.21}$$

Ever since the power extracted from the second disc does not affect the first disc, for the maximum total $C_P = C_{P1} + C_{P2}$, C_{P2} must have the maximum value. $dC_P / db = 0$, then $b = 1/3$.

Then, the maximum value of total power coefficient is gained by the differentiating the equation

$$\frac{dC_{P1}}{da} + \frac{dC_{P2}}{da} = 0. \tag{2.22}$$

Then, $a = 1/5$.

From the derivation, the maximum value is

$$C_{P_{\max}} = C_{P1} + C_{p2} = \frac{64}{125} + \frac{16}{125} = \frac{16}{25}. \tag{2.23}$$

Moreover, in case of N actuator in series, interference coefficients which make maximum coefficient condition are inductively $1/(2N+1)$, $1/(2N-1)$, $\cdots$, 1/3 (From upstream to downstream at each disc). Now we can calculate the maximum value of total power coefficient of N actuator discs in series. It follows

$$C_{P_{\max}} = \frac{8(1+(1/N))}{3(2+(1/N)^2)}. \tag{2.24}$$

For $n \to \infty$, $C_P = 2/3$. It converges to its limit very fast.

3. Turbine Modeling

The Transverse Horizontal Axis Water Turbine (THAWT) is modeled with 3-blades which are located in the same distance from the rotation axis operated under the linear velocity gradient. At first, dimensional analysis for a flow and the turbine is conducted. Then, the derivation of turbine model is simplified under some assumptions and the equation of motion is actually given as analytic form. Nevertheless, it should be solved numerical way from the lift and drag coefficients, which depend on the shape of blade and its corresponding Reynolds number.

3.1. Dimensional analysis

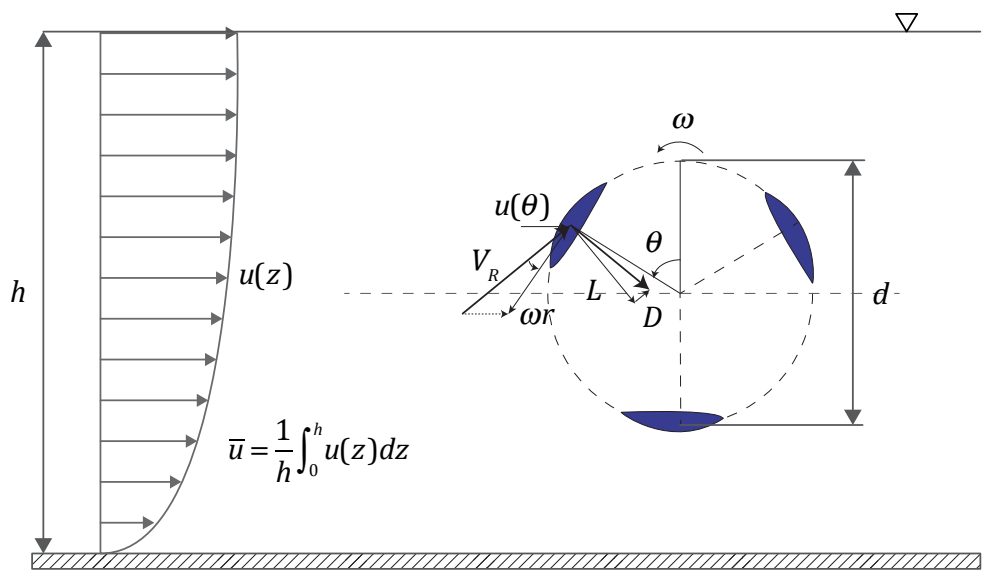

Fig. 15. Schematic figure for the typical case of tidal turbine with some representative variables

A simple application of dimensional analysis helps to construct model and design criteria. From the Fig. 15, we can check the operational condition of the target turbine. The important variables considered in this model are listed in Table. 1. Note that although the figure is drawn as two-dimensional schematic, it is actually stretched form for lateral direction with the lateral length L also included in variables.

Table. 1. The name of variables, symbols and its dimension for modeling THAWT

Variables	**Symbol**	**Dimension**
Generated power per unit length	P	$\left[M/T^3\right]$
Lift force per unit length	L	$\left[M/T^2\right]$
Drag force per unit length	D	$\left[M/T^2\right]$
Pressure difference between local and vapor pressure	Δp	$\left[M/LT^2\right]$
Surface tension	σ	$\left[M/T^2\right]$
Density of fluid	ρ	$\left[M/L^3\right]$
Gravitational acceleration	g	$\left[L/T^2\right]$
Kinematic viscosity	ν	$\left[L^2/T\right]$
Relative blade velocity	V_R	$\left[L/T\right]$
Blade component velocity	$\omega r = \omega d/2$	$\left[L/T\right]$
Mean flow velocity	$\bar{u}$	$\left[L/T\right]$

Velocity gradient	du / dz	$[1/T]$
Diameter of turbine	d	$[L]$
Water depth	h	$[L]$
Width of turbine	w_d	$[L]$
Chord length of blade	c	$[L]$
Angle of attack	α	-

There are 17 variables and 3 basic dimensions. Therefore, 14 dimensionless groups are required to represent this system. Using the dimensional analysis, the list of dimensionless groups is derived as the table below. Note that some variables are used instead of representative values to express the dimensionless parameters in a physically meaningful way. For example, the relative blade velocity is used instead of upstream mean flow velocity to calculate the lift and drag coefficient. Also, instead of using the velocity ratio between relative velocity and mean flow velocity, the blade Reynolds number is adopted by combining with another dimensionless parameter (Blockage ratio).

Table. 2. Dimensionless group, symbols and corresponding variables

Variables	Symbol	Variables
Power coefficient	C_P	$P/\left(\frac{1}{2}\rho u^3 d\right)$
Lift coefficient	C_L	$L/\left(\frac{1}{2}\rho V_R{}^2 c\right)$
Drag coefficient	C_D	$D/\left(\frac{1}{2}\rho V_R{}^2 c\right)$
Cavitation number	C_a	$\Delta p / \rho c^2$
Weber number	We	$\rho V_R{}^2 c / \sigma$
Reynolds number: flow	Re_f	$\bar{u}h/\nu$
Reynolds number: blade	Re_b	$V_R d/\nu$
Froude number	Fr	$u/\sqrt{gh}$
Tip speed ratio	λ	$\omega d/2\bar{u}(=\omega r/\bar{u})$
Relative velocity gradient	V_G	$d\left(du/dz\right)/\bar{u}$
Blockage ratio	B	d/h
Relative lateral length	w_{d_d}	w_d/d
Chord to diameter	c_d	c/d
Angle of attack	α	-

Note that we already have the relationships between some variables. For example, lift and drag coefficients are related to the blade Reynolds number and angle of attack from previous blade element momentum theory discussed in 2.3.

3.2. Derivation of simplified model

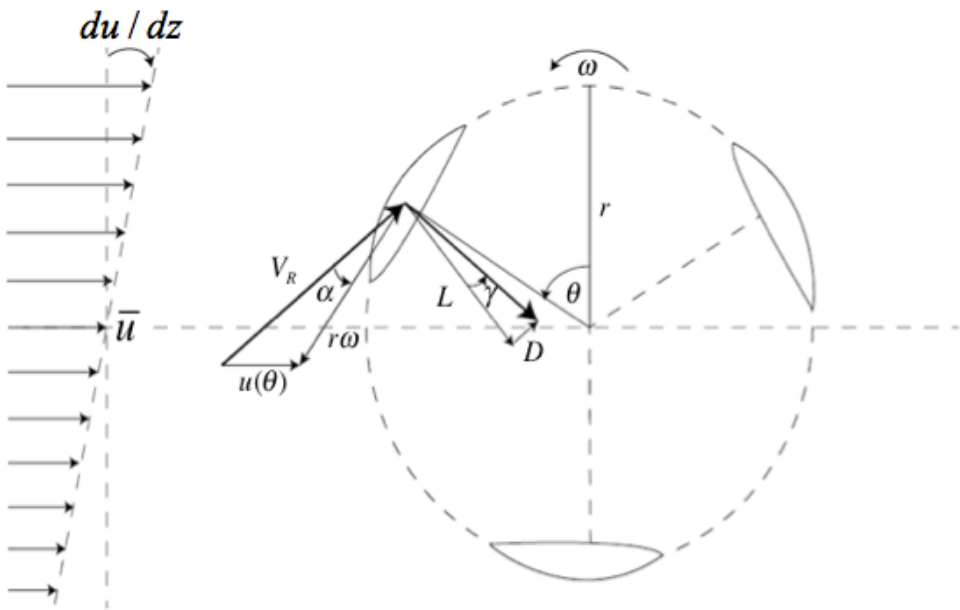

Fig. 16. 3-Blades Darriues type turbine with linear velocity profile

Assume that the flow is steady and uniform, while the turbine blades do not disturb upstream flow field. The 3-Blades Darrieus type turbine can be simplified as the combination of 3 hydrofoils, which have same shape and distance from the axis. Assume the oncoming velocity of flow has only x-directional component. Then, the velocity vector acting on each blade at θ is defined as

$$\vec{u} = (u(\theta), 0) \tag{3.1}$$

$$u(\theta) = \bar{u} + \frac{du}{dz} r\cos\theta = \bar{u}\left(1 + \frac{r(du/dz)}{\bar{u}}\cos\theta\right) \tag{3.2}$$

where the vertical mean velocity of the flow is $\bar{u}$ and the linear velocity gradient is du/dz.

From the oncoming flow for steady velocity profile $u(\theta)$, the relative velocity between the flow and each hydrofoil with angular velocity ω is related to analyze the efficiency and its motion. The relative velocity vector and its magnitude can be defined as

$$\vec{V}_R = (u(\theta) + r\omega\cos\theta, r\omega\sin\theta) \tag{3.3}$$

Now, the angle of attack α is used to obtain the lift and drag force, which cause the rotation of turbine and generate energy. α is defined as the angle between the relative velocity vector $\vec{V}_R$ of the flow and the tip speed $r\vec{\omega}$ of hydrofoils where $\vec{\omega} = (-\omega\cos\theta, -\omega\sin\theta)$. Then,

$$\cos\alpha = \frac{(u(\theta)\cos(\theta) + r\omega)}{\left|\vec{V}_R\right|} \tag{3.4}$$

The lift force is perpendicular to the resultant velocity vector and the drag force is parallel to the resultant velocity vector. For chord length of hydrofoil c. C_L for lift and C_D for drag, the lift and drag force for unit length can be defined as

$$L = \frac{1}{2}\rho {V_R}^2 c C_L \tag{3.5}$$

$$D = \frac{1}{2}\rho {V_R}^2 c C_D \tag{3.6}$$

On the other hand, the weight of hydrofoil also affects to the force equilibrium based on the position of each blade. Therefore, the total force F acting on turbine is the combination of lift, drag, and gravitational forces. Assume that each hydrofoil is well locked up for its direction to their axis, by combining the lift, drag and gravity force.

The net force F for tangential and normal direction is

$$(F_T)_i = (L\sin\alpha - D\cos\alpha)_i + (mg\sin\theta)_i \tag{3.7}$$

$$(F_N)_i = (L\cos\alpha + D\sin\alpha)_i + (mg\cos\theta)_i \tag{3.8}$$

where i is the numbering of each hydrofoil. In this 3-blade case, for $i = 1, 2, 3$.

The weight of turbine is obtained by considering buoyancy effect,

$$m = (\rho_b - \rho)V \tag{3.9}$$

Note that ρ_b is density of blade.

We can neglect the gravity term by equally spaced blade.

$$\sum (F_T)_i = \sum (L\sin\alpha - D\cos\alpha)_i + \sum (mg\sin\theta)_i = \sum (L\sin\alpha - D\cos\alpha)_i$$

$$\because \sum (mg\sin\theta)_i = mg\sum (\sin\theta)_i$$

$$= mg\left[\sin(\theta_1) + \sin(\theta_2) + \sin(\theta_3)\right]$$

$$= mg\left[\sin(\theta_1) + \sin(\theta_1 + \frac{2}{3}\pi) + \sin(\theta_1 + \frac{4}{3}\pi)\right]$$

$$= 0$$

Same for normal force

$$\sum (F_N)_i = \sum (L\cos\alpha + D\sin\alpha)_i + \sum (mg\cos\theta)_i = \sum (L\cos\alpha + D\sin\alpha)_i$$

$$\because \sum (mg\cos\theta)_i = 0$$

Therefore, the net force F for tangential and normal direction is

$$(F_T)_i = (L\sin\alpha - D\cos\alpha)_i \tag{3.10}$$

$$(F_N)_i = (L\cos\alpha + D\sin\alpha)_i \tag{3.11}$$

For very small-time change dt , we can define the angular velocity of turbine from force equilibrium.

$$m \cdot \frac{d(\omega r)}{dt} = \begin{cases} 0 & (\sum F_T \le \mu_s F_N) \\ (\sum F_T - \mu F_N) & (\sum F_T > \mu_s F_N) \end{cases}$$

or

$$\frac{d\omega(t)}{dt} = \begin{cases} 0 & (\sum F_T \le \mu_s F_N) \\ \dfrac{\sum_{i=1}^{3} F_T - \mu F_N}{mr} & (\sum F_T > \mu_s F_N) \end{cases} \tag{3.12}$$

where μ_s is friction of rest.

The location of each blade is

$$\frac{d\theta_i(t)}{dt} = \omega(t) \tag{3.13}$$

and

$$\theta_i(t) = \theta_i(0) + \int_0^t \frac{d\theta}{dt}\,dt = \int_0^t \omega(t)dt \quad (for\ \ i = 1,2,3) \tag{3.14}$$

The power is obtained from

$$P(t) = F(t) \times V(t) = \sum_{i=1}^{3} F_i(t) \times r\omega(t) \tag{3.15}$$

Total generated energy is obtained from

$$E(t) = \int_0^t P(t)dt = \int_0^t \sum_{i=1}^{3} F_i(t) \times r\omega(t)dt \tag{3.16}$$

Also, the power coefficient is

$$C_p = \frac{P(t)}{\frac{1}{2}\rho u^3 A} = \frac{\sum_{i=1}^{3} F_i(t) \times r\omega(t)}{\frac{1}{2}\rho u^3 (2r)} \tag{3.17}$$

Although the solution takes closed form, the time varying solution of equation 3.17 is obtained from numerical method by solving equation 3.12 and 3.13 because of there is no closed-form of lift and drag coefficient for arbitrary shape of blade. Fortunately, the simplicity of governing equation of motion (equation 3.12) can be solved in finite difference method which leads to the usage of numerical scheme guaranteeing higher order accuracy and stability such as the 4^{th} order Runge-Kutta method.

3.3. Calculation Procedure

The ordinary differential equations 3.12 and 3.13 in section 3.2 are solved in the following procedures. The parameters for the numerical calculation is listed below.

i) Fluid properties: density, kinematic viscosity, water depth, and velocity profile

ii) Turbine properties: density of material, diameter, chord length of blade, and friction coefficients between materials

iii) Numerical setup: time step, initial positions of each blades, and initial angular velocity of turbine

Now, the solving procedures are followed as below.

i) Determine the fluid velocity acting on the blade using equations 3.1, and 3.2

ii) Using equation 3.3, get relative velocity of fluid acting on the blade. Also, the angle of attack is given from equation 3.4.

iii) Calculate the lift and drag forces from equation 3.5 and 3.6. Note that the lift and drag coefficient is derived from blade Reynolds number and angle of attack from the experimental data given in chapter 2.3.

iv) From lift and drag force, decompose them to the tangential and normal force by using 3.10 and 3.11.

v) Obtain the new angular velocity from equation 3.12, and update the location of blade from 3.13.

vi) By combining the steps from i) to v), the single augment of calculation is finished. We can apply the multi-step numerical method including predictor and corrector from repeat of them. For each augment, the generated energy and power coefficient is given from 3.16 and 3.17.

In Fig. 17, the calculation procedure is arranged in flow chart.

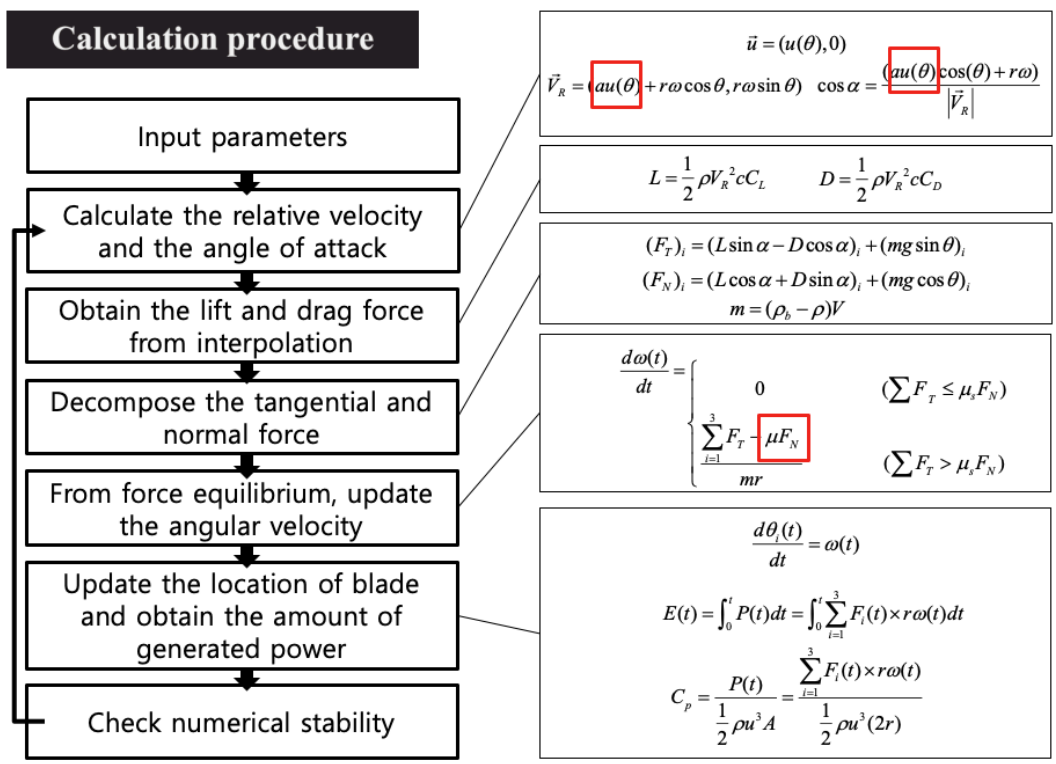

Fig. 17. Procedure for the model calculation

Note that in Fig. 17, the red boxes show some adjust coefficient used in numerical code.

$$\vec{V}_R = (a \times u(\theta) + r\omega\cos\theta, r\omega\sin\theta) \tag{3.18}$$

$$\frac{d\omega(t)}{dt} = \begin{cases} 0 & (\sum F_T \le \mu_s F_N) \\ \dfrac{\sum_{i=1}^{3} F_T - \mu F_N}{mr} & (\sum F_T > \mu_s F_N) \end{cases} \tag{3.19}$$

The equation (3.18) gives the velocity induction factor a which indicates the decreasing velocity while the flow is located at the blade based on the LMADT concept given in part 2.2. The friction factor μ is suggested in equation (3.19) and it means the frictional effects based on its normal directional force. These two variables are applied to adjust the model based on experimental work. The effect of them will be discussed in part 3.4.

3.4. Numerical results

Table. 3. Fixed* parameters for numerical solution

Input parameters	Values
Diameter of turbine	0.05 m
Density of fluid	1,000 kg/m^3
Density of blade	1,250 kg/m^3
Water depth	0.10 ~ 0.30 m
Gravitational acceleration	9.81 m/s^2
Chord length of blade	0.02 m
Width of blade	0.0024 m
Initial time step	0.01 s*

* For stability, time step can be changed for each calculation step.

In Table. 3, the input parameters used in numerical simulation for sample results are given. The density of blade is the typical density of blade to match with the material used in experiment, 3-D printer ink, PLA. Note that the time step is given in initial time step, which indicates that it can be changed for each numerical step. If the location of blade is changed more than 1-cycle during the single time step, the stability problem is occurred in numerical calculation. To prevent them and enhance the model, the time step changing code is inserted in numerical calculation. In Fig. 18, the example of changing time step for stability issue is given and the numerical solution converges very fast and well to its equilibrium condition as the trend shown in Fig. 19. Now, the sample results for ideal case which means

no velocity induction and zero friction ($a = 1$ and $\mu = 0$) in same mean upstream velocity $u = 0.1\text{m/s}$.

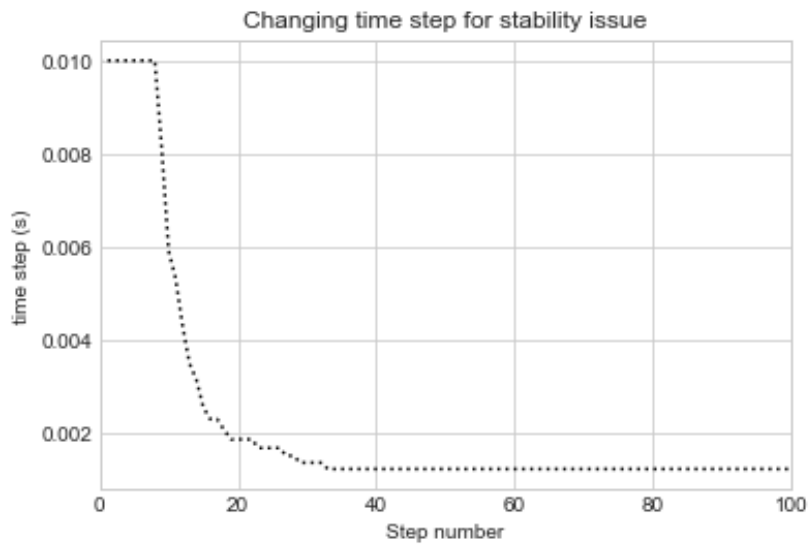

Fig. 18. Example of changing time step for numerical stability

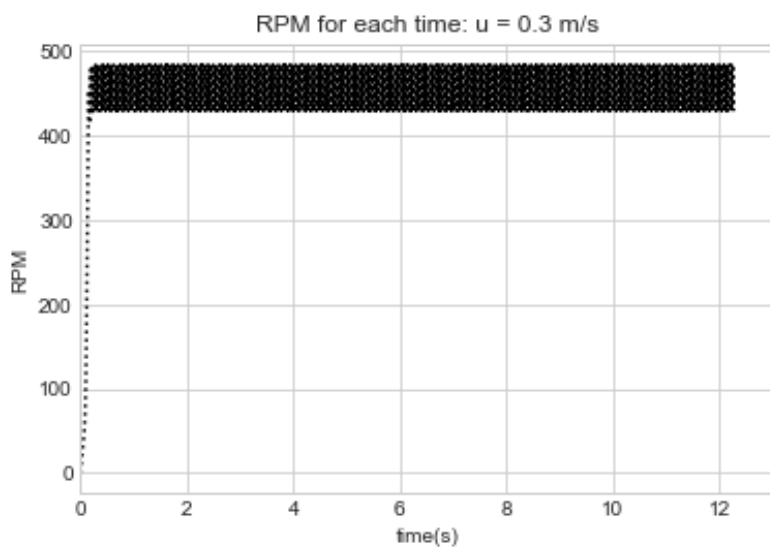

Fig. 19. RPM at each time until equilibrium condition

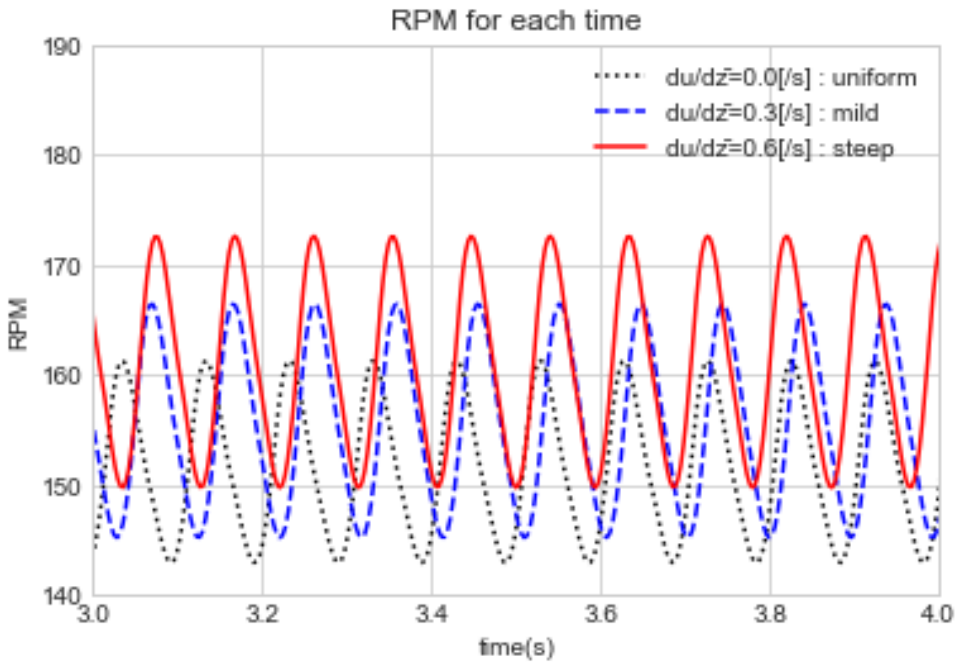

Fig. 20. RPM for ideal case with various velocity gradient

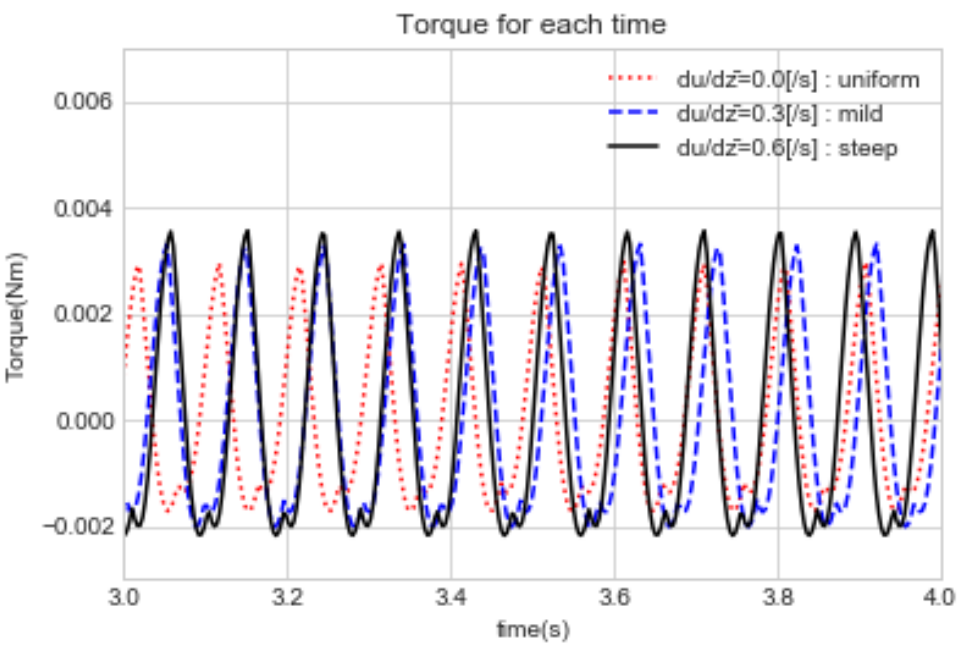

Fig. 21. Torque at each time for ideal case with various velocity gradient

In Fig. 20 and 21, the RPM and torque for each time is given after it converges to the equilibrium condition. Note that the mean RPM and torque increase for the 'steep' gradient which gives the larger velocity gradient values. It leads that the presence of the velocity gradient can affect the force acting on the blades and change the rotational speed of the turbine motion.

In Fig. 22, each line indicates the change of power coefficient at each equilibrium cycle in a given mean velocity. The x-axis notes the tip speed ratio $\omega r / \overline{u}$ that the ratio between the tip speed of blade and the upstream flow velocity. We can easily check that the turbine has large power coefficient as the mean velocity increases. Also, the higher power coefficient can be obtained for higher tip speed ratio $\omega r / \overline{u}$. From this, it is important to keep higher tip speed ratio in uniform flow to obtain the more amount of energy.

Fig. 23 also shows that the amount of generated power is increased for steep velocity gradient. However, it is also noted that the relative increment is less than the figure 18. The case of solid black line indicates that the flow velocity at lowest part of fluid is almost zero which is very ideal case. Therefore, to increase the total energy generated by turbine, the effect of large mean velocity and presence of velocity gradient might have powerful influence to the expected results.

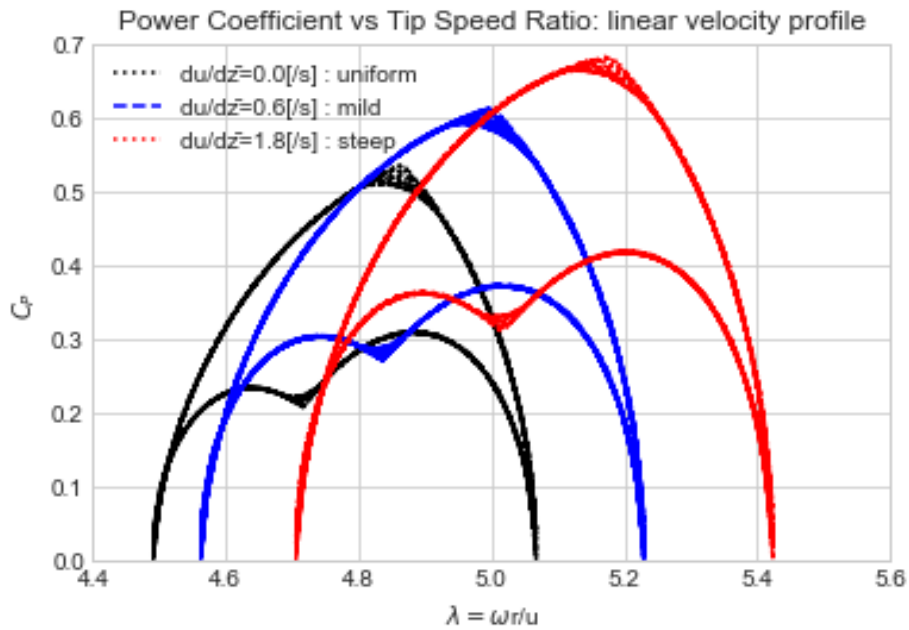

Fig. 22. Power coefficient vs Tip speed ratio for ideal case with various velocity gradient

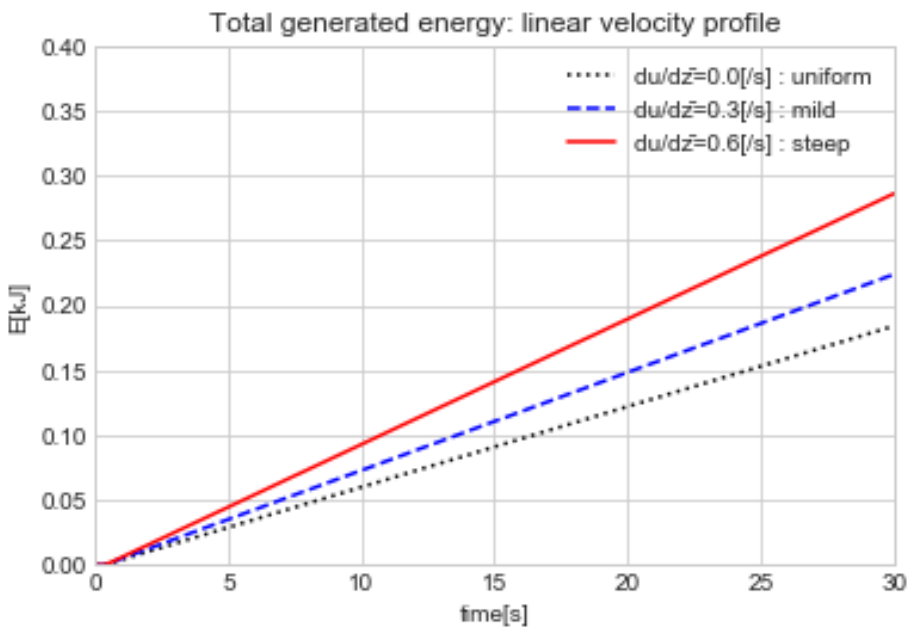

Fig. 23. Total generated energy for ideal case with various velocity gradient

On the other hand, the model can be adjusted by applying the LMADT concept suggested in chapter 2 and friction coefficient considered in the two equations (3.18) and (3.19). The results in Fig. 24 and 25 clearly show the tendency of adjusting two parameters. The velocity induction factor diminishes the RPM and do not affect the fluctuation of turbine, while the friction factor also diminished the RPM making larger fluctuation.

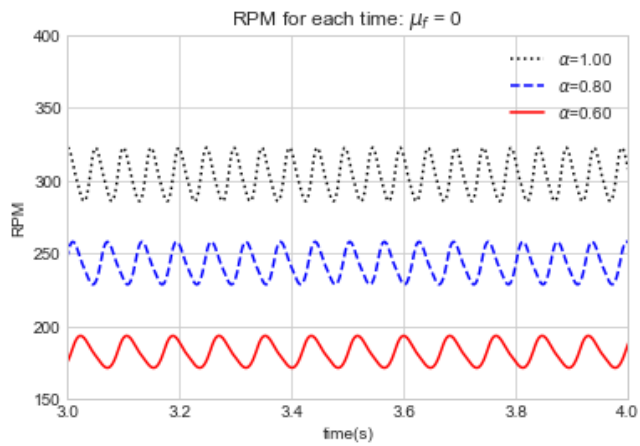

Fig. 24. RPM of model for $\mu = 0$

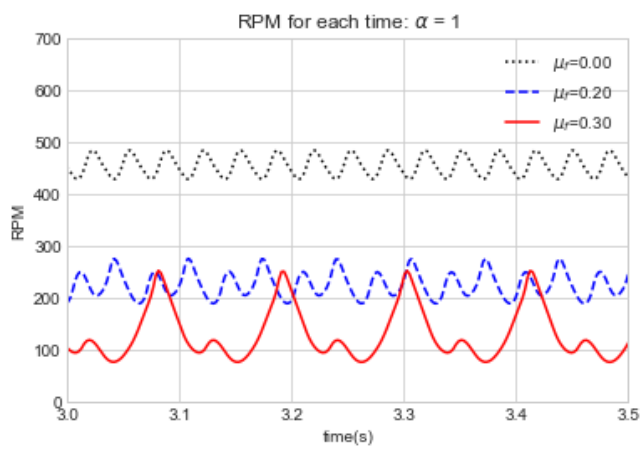

Fig. 25. RPM of model for $a = 1$

4. Experimental Setup

In this section, several descriptions for experiment will be conducted to validate and calibrate the result of simplistic model. At first, the flow condition of flume is confirmed from dimensional analysis by comparing the parameters discussed in previous study. Then, the method of flow velocity field measurement by using Vectrino will be discussed for its properties and uncertainties. Also, scaled modeling of turbine device is introduced with some comments. Finally, simple image processing techniques to capture the rotational motion of small turbine is introduced.

4.1. Similitude and flow conditions

Fig. 26. Picture of flume

The flume used in this experiment is the open channel flume. At the midpoint of channel, the bottom is clear that makes the light such as laser can penetrate it. The length of channel is 4600 mm, width is 300 mm, height is 500 mm. The limitation of operating height (200 mm) of flume is from the channel junctions for 25 mm height and relatively low flow rate. From the real-time operation of pump, the flow rate of this channel is recorded as 6.7 ~ 420 l/min . Among various dimensionless numbers, the primary and easily applicable factors are Reynolds number and Froude number.

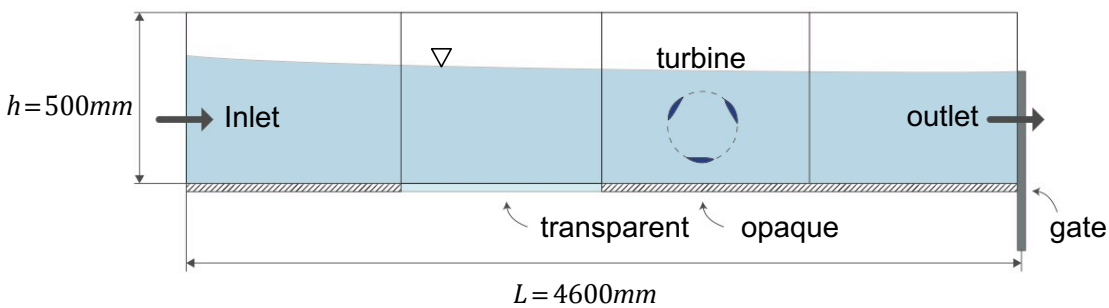

Fig. 27. Schematic diagram of flume

In real application, the typical diameter of THAWT is given as 10~20 m operated in a flow depth of 20~50 m, and the lateral length of each rotor is 40~80 m long (McAdam, 2011). Now, we can simply set the magnitude of mean water velocity of this area given as 0.35 m/s (standard deviation is 0.09 m/s) and the maximum velocity as 3.76 m/s. The representative non-dimensional numbers between model and prototype in this research is suggested below.

In experiment, the possible operation of mean water velocity is $5.0\times10^{-2} \sim 3.0\times10^{-1}$ m/s. Note that we can set the experiment for operating in the sense of Froude similarity. However, it is hard to accurately match the Reynolds number since the flow rate and size of this flume is relatively small. Therefore, the experiment will be operated in large flow rate as much as possible to fulfill the high turbulent condition in original operating condition. The representative variables in model and prototype are suggested in table below. Other variables have same quantity in both conditions such as gravitational acceleration, kinematic viscosity, etc.

Table. 4. Representative variables in prototype and model

Range of conditions	**Prototype**	**Model**
Water velocity (m/s)	0.15 ~ 0.45	0.05 ~ 0.30
Water depth (m)	20 ~ 50	0.1 ~ 0.2
Diameter of turbine (m)	10 ~ 20	0.05 ~ 0.07

Now, 4 representative non-dimensional parameters are selected and discussed to deal with the similarity issues between prototype and model. First, the blockage ratio (B), which is the ratio between the water depth and the diameter of turbine, is 0.2~0.5 in prototype while 0.3~0.7 in the model. It simply says about the geometric similarity between them. Second, the Reynolds number (Re), which is determined by the mean velocity, water depth as characteristic length, and kinematic viscosity,

is more than 70,000 in prototype and exceed 5,000 in model. Although the range of Reynolds number is not matched well, it is quite enough to have fully turbulent flow in both conditions. Third, the Froude number (Fr), is calculated from mean velocity, and water depth as characteristic length, and gravitational acceleration. In prototype, it has 0.016~0.024 while 0.010~0.049 in model condition. It has benefit of considering wider range of Froude number than prototype and containing the range of prototype condition. Finally, the Weber number (We) is more than 30,000 in prototype and 33 in model. Since it fulfills the condition $We>>1$, the effect of surface tension will be easily neglected.

4.2. Velocity measurement

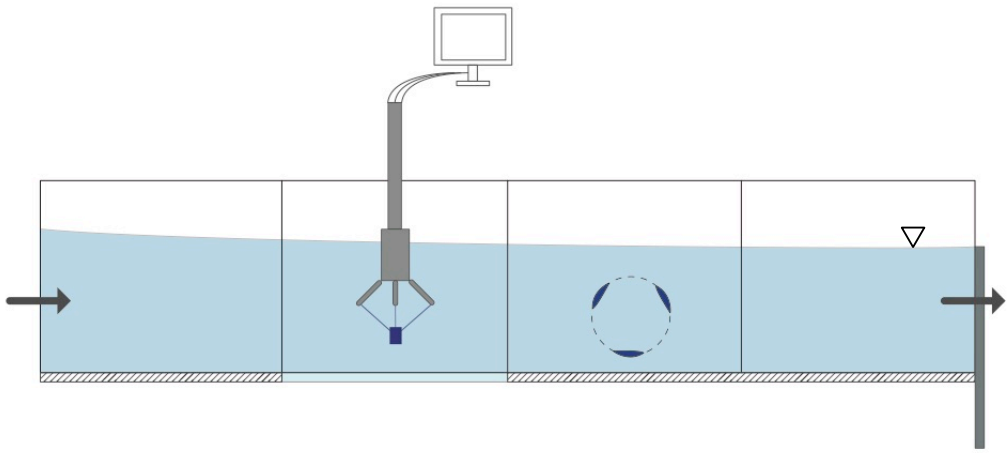

Fig. 28. Schematic diagram of velocity measurement using Vectrino

In this experiment, the velocity measurement of the flow field will be conducted by using Vectrino. Vectrino is the device to capture the instantaneous velocity components at a specific given point. It actually measures the velocity of particles in a sampling volume based on the Doppler effect (Voulgaris & Trowbridge, 1998). Nortex Vectrino I which is a single-point measurement will be used in this research. It is widely used in 3D flow measurements in laboratory flumes and inexpensive than laser Doppler velocimetry (Nortek, 2009). This device consists of one central transducer which transmits the acoustic sound waves to the sampling volume and four receivers which receive the reflected (also shifted in frequency sense) waves by the particle inside the sampling volume. The measured phase shift is

proportional to the velocity of particle from the Doppler effect. More detail specifications of the Vectrino I are following below.

Table. 5. Specifications of Nortek Vectrino I

Specifications	**Values**
Distance from probe	50 mm
Sampling volume diameter	6 mm
Sampling volume height	3 ~ 15 mm
Velocity range	± 0.01 ~ 4 m/s *
Sampling rate	1 ~ 200 Hz
Accuracy	± 0.5 % of measured value ± 1 mm/s
Operating temperature **	-4 ~ 40 °

* The velocity range is not the same in the horizontal and vertical direction.

** Thermistor embedded in probe.

Although its effectiveness to simply measure the fluid velocity, there are limitations. First, it needs to supply the sufficient particles or be applied in the turbidity flow for capturing the velocity of particles. Note that the number of particles should not affect the conditions of carrier fluid. Also, it will be operated under the condition is valid that the particles resemble the movement of the flow particle. Furthermore, it starts to measure the velocity 50 mm below the surface elevation since its sampling volume is located 50 mm below from the transducer.

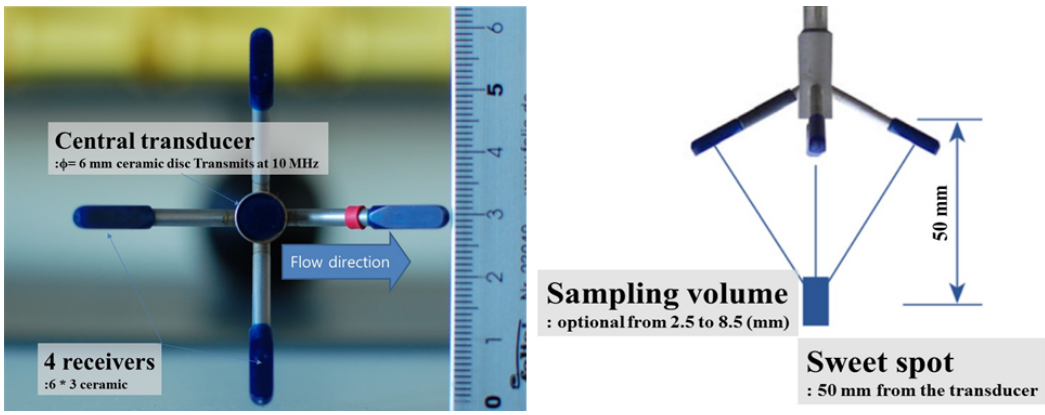

Fig. 29. Schematic diagram of Vectrino I (Nortek, 2009).

By considering the limitation of operating height (200 mm) of flume, the operating depth of Vectrino is now up to 150 mm from bed. To capture the dramatic velocity change for near-bed condition and consider the relatively uniform shape of vertical profile, the distance between measurement points will be finer near bottom than close to surface. For example, we can simply choose the measuring points by following an arithmetical progression as 3, 5, 8, 12, 17, 23, 30, 38, 47, 57, 68, 80, … as follows.

Before capturing the actual usage of velocity profile and the flow development along the flume, the number of measuring points and sampling rate should be determined in an effective and accurate way. Note that the number of sampling points determines the accuracy of the vertical velocity distribution, and the sampling rate determines the minimum capturing periodic components of velocity which capture the turbulent characteristics of flow.

Although the more measuring points and the higher sampling frequency lead the better result, we don't need to increase the points or using high frequency option if the results cannot show the notable or meaningful improvement after that. Therefore, by starting from the highest frequency and sufficient number of measuring points, the minimum frequency will be determined first to capture the mean flow velocity at a point ergodic in time scale. Then, the number of points will be discussed to represent the velocity profile well. Now, the velocity measurements from Vectrino is conducted and summarized below.

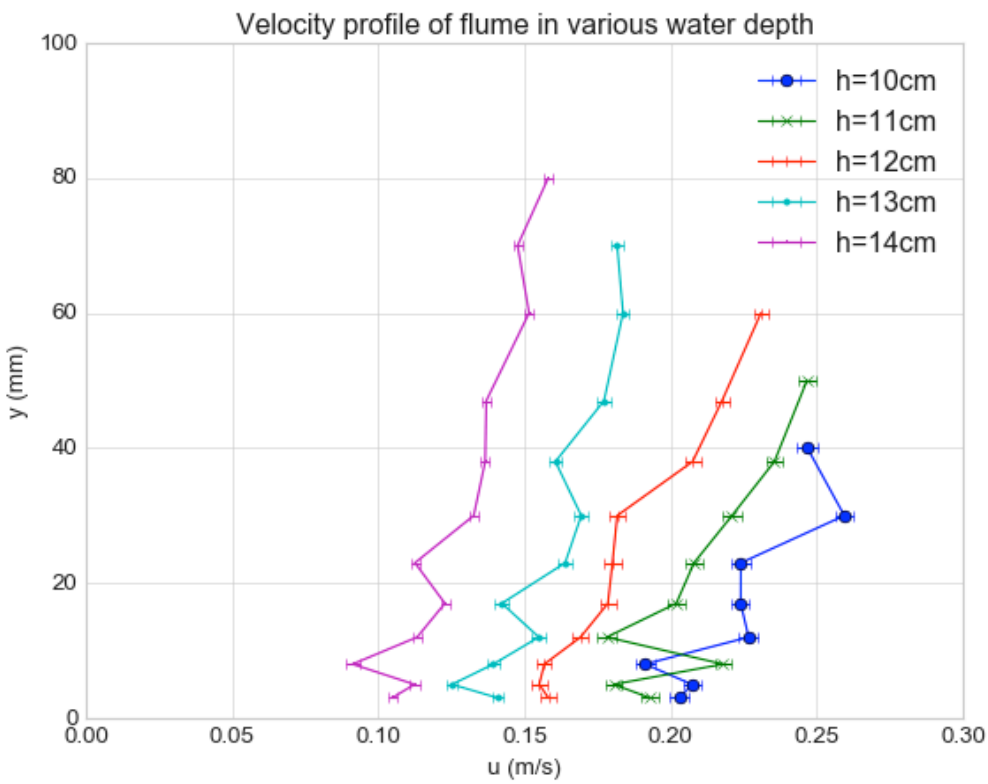

Fig. 30. Velocity profile of flume in various water depth.

The velocity profile of flume was measured by Vectrino. The Fig. 30 shows the mean velocity of water at specific point with confidence level of 95% based on t-test. These results will be applied directly to the numerical model to calibrate the model coefficients with experimental results. Note that we will discuss x-directional velocity which is perpendicular to the rotational axis of turbine since the simplified model derived in section 3 assumes the 2-D condition with zero vertical velocity. Also, the mean vertical velocity has much smaller values than the x-directional velocity in this experiment flume.

4.3. Making small-scale turbine

The small-scale turbine model is made by the 3D-printer; MakerBot. It makes the 3D object file made by design programs such as AutoCAD into the real object made by PLA ingredient. There are some procedures to make the device properly in this research.

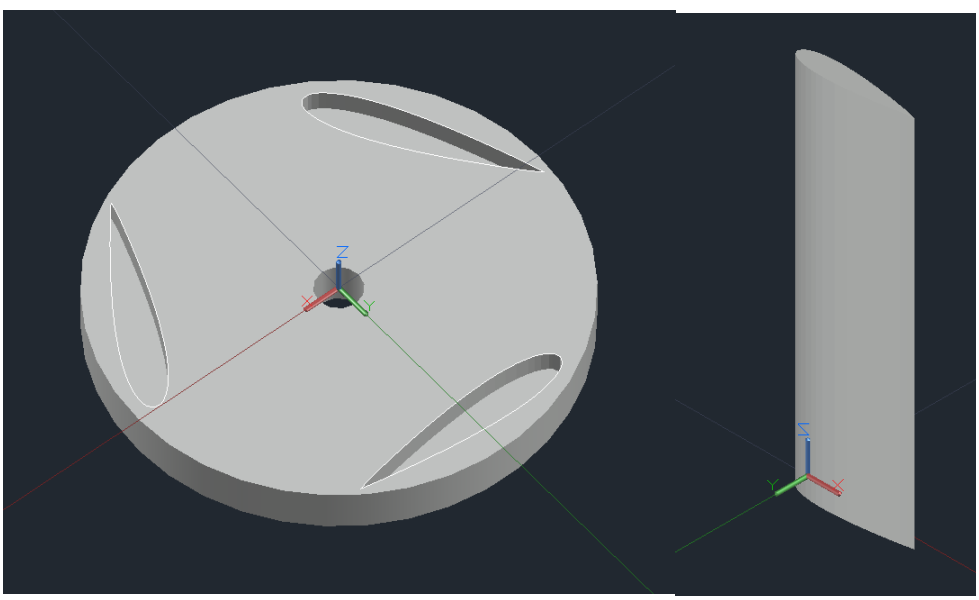

Fig. 31. Turbine module designed by CAD. (left) Fixed plate, (right) Blade

The Fig. 31 shows the AutoCAD design module to make turbine as self-assembly. While it is also possible to print the object directly in full-scale model, it is not available to support the 'floating' part of turbine which makes the quality of output lower. To deal with this issue, the self-assembly design is selected and print the turbine by parts.

On the other hand, each object should be printed separately even if we can put them into single project file in 3D printer. It is because of the inner problem of 3D printer that when we print the multiple objects in same time, the objects which is far from the center are printed thinner than we expected. Fig. 32 and 33 show the example of usage of 3D printer.

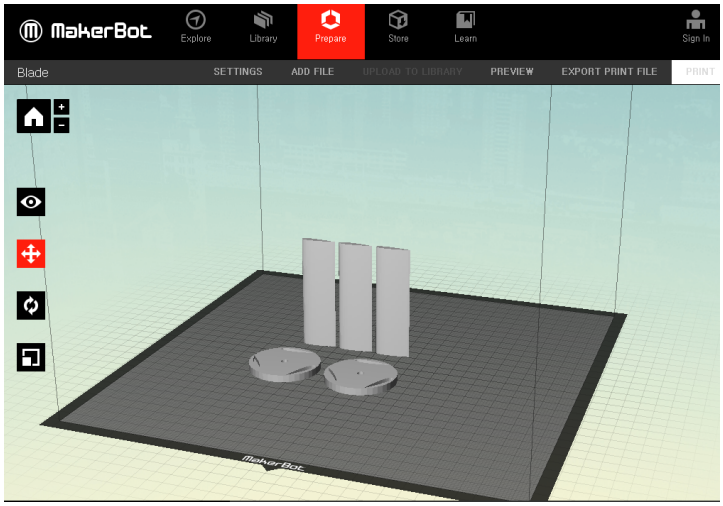

Fig. 32. Example of using 3D printing program; MakerBot

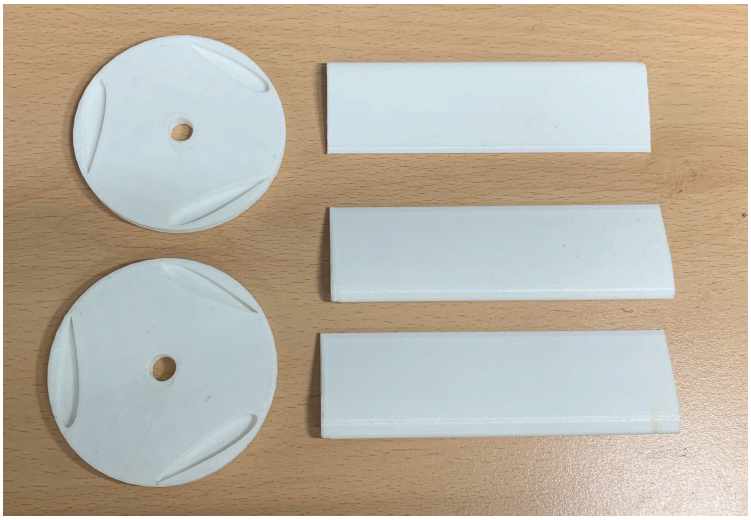

Fig. 33. Result of 3D printing, 2 plates and 3 blades; D = 7cm

4.4. Measuring motion of turbine

To validate the simplified model derived in chapter 3, the quantifying procedures of experimental device are suggested in this chapter. Except the flow conditions such as velocity or water depth, there are two important variables which have issues about measuring and validating of model; torque and angular velocity. In this research, the angular velocity will be discussed as the main output parameters of turbine device. Since the main factor of generator installed in turbine is the RPM which indicates the rotational speed of device, it will be enough to discuss only about the angular velocity of turbine modules in experiment. The motion of turbine is measured and captured by the simple image processing with following procedures.

Table. 6. Specifications for image video

Specification	Values
Frame	30 /sec
Size	720 x 1280 pixels
Measuring time	1 min
Repetition	5 times
Color format	HSV
Range of color	Red: [160, 50, 50] ~ [179, 255, 255] Blue: [90, 50, 50] ~ [120, 255, 255]
Measurement limit	0.0033 mm/s

The first step is extract object from image or video. The size of video is 720 x 1280 pixels with 30 frames per second. The target color is extracted from HSV color scale which matches well into the visual condition of our eyes rather than RGB scale. For example, the red color in HSV is from near [160, 50, 50] to [179, 255, 255]. Also, it can be changed case by case. The extracted data is based on the python open-cv2, mask forms which is also 720 x 1280 matrix and has 0 or 255 values based on its information.

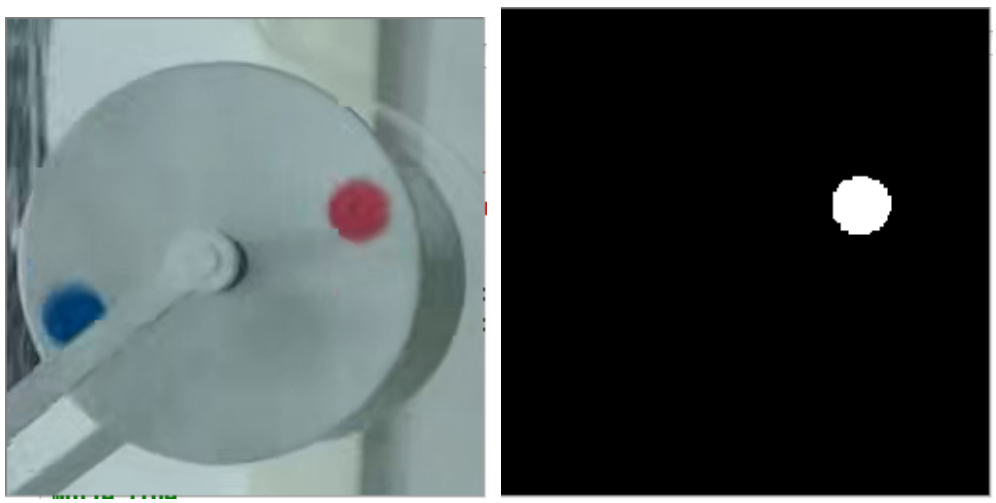

Fig. 34. Example of extracted image of center of the circle attached in turbine

After we get the mask matrix, the position of center of circle should be derived to obtain the quantified values. Let converting matrix as below

$$Nb = \frac{1}{255}\begin{bmatrix} 1 \\ 1 \\ ... \\ 1 \end{bmatrix}_{1280\times 1} \tag{4.1}$$

Then, the number of points in mask matrix is derived from the relation

$$\text{Mask}_{720\times 1280} \cdot Nb_{1280\times 1} = \begin{bmatrix} 1 \\ 0 \\ ... \\ 1 \end{bmatrix}_{720\times 1} \tag{4.2}$$

Then, the center of circle is simply

$$Rc = \frac{1}{255}\begin{bmatrix} 1 \\ 2 \\ ... \\ 1280 \end{bmatrix}_{1280\times 1} \tag{4.3}$$

$$Lc = \frac{1}{255}\begin{bmatrix} 1 \\ 2 \\ ... \\ 720 \end{bmatrix}_{720\times 1} \tag{4.4}$$

Then, the sample results are followed as below.

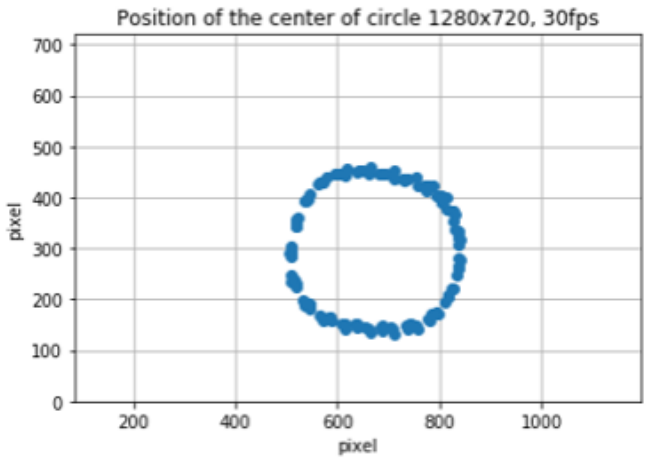

Fig. 35. Example of extracted center of the circle attached in turbine

By simply matching them into circle, the radius and center of the turbine in image is derived.

The least square method is applied in this section.

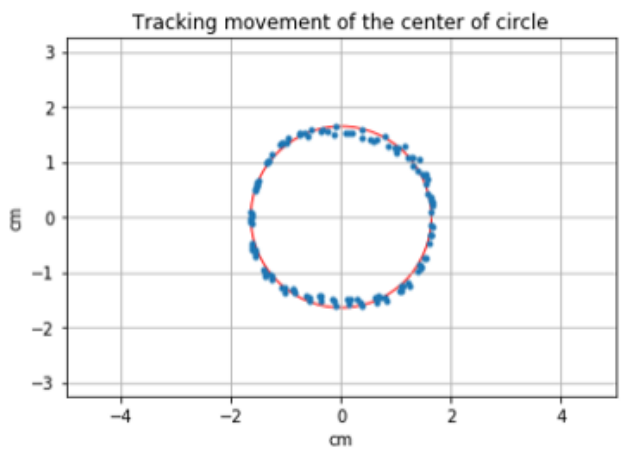

Fig. 36. Tracking movement of the center of circle with real size.

Now, the position of circle at each time is calculated based on

$$x - X = r\cos\theta$$
$$y - Y = r\sin\theta$$

Then,

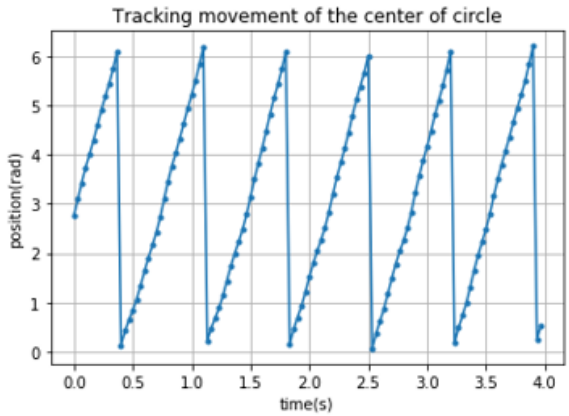

Fig. 37. The position of attached circle at each time based on angle

By converting into RPM with the equation,

$$\Delta\theta \times fps \times 60 = RPM$$

the angular velocity converted into RPM is calculated as below.

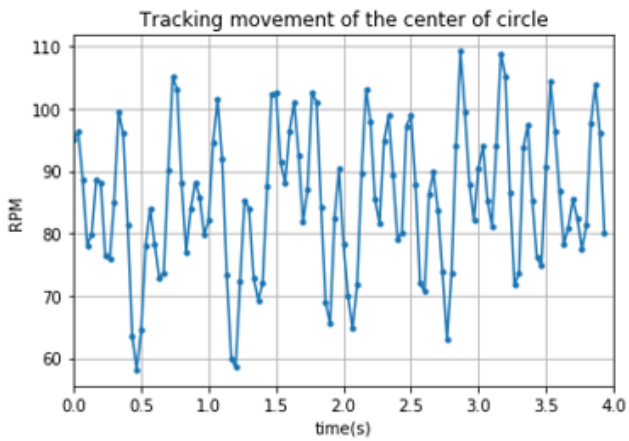

Fig. 38. Example of angular velocity of turbine converted into RPM

5. Results and discussion

5.1. Experimental results

By using the method given in section 4, the angular velocities for various size of turbine are obtained from experimental work. The results based on the non-dimensional number are given below.

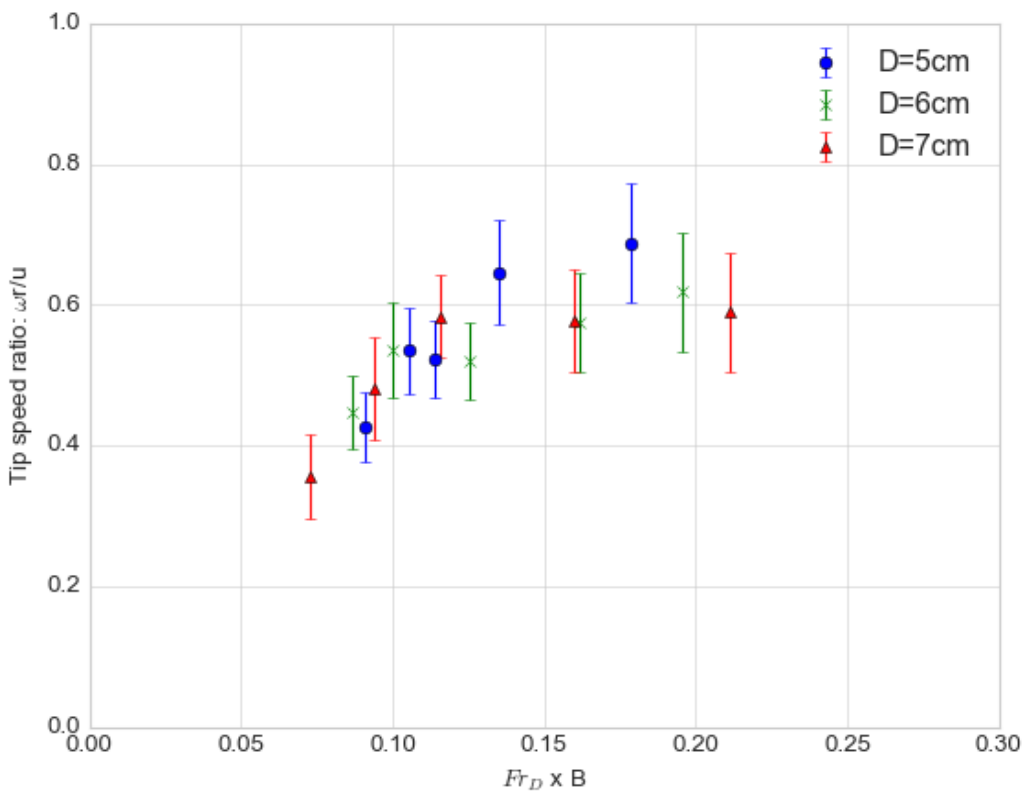

Fig. 39. Tip speed ratio vs. Turbine Froude number x Blockage ratio on various turbine size

Note that there are the newly suggested non-dimensional variables defined as

$$\mathrm{Fr}_D = \frac{u}{\sqrt{gD}}. \tag{4.5}$$

It is turbine Froude number which choose the diameter of turbine as its characteristic length. The product of turbine Froude number and Blockage ratio is in x-axis while the tip speed ratio is given in y-axis. It is chose based on its clear trend while the various combination of parameters used in experimental work.

In Fig. 39, the error range is determined by the 95% confidence level with t-test based on 5 times of repeat experiment. For various number of non-dimensional parameters, the variables should have information about water depth, angular velocity, mean velocity, and size of turbine. Among them, the relationship between tip speed ratio and turbine Froude number x Blockage ratio shows the clear trend. It shows that for fast mean velocity and relatively larger turbine size than water depth leads to the fast-rotational speed. However, in the simplified model, the tip speed ratio has only upper limit with constant values near 4 ~ 5, since it is exaggeratedly idealized model. Therefore, the model calibration should be conducted based on the experimental results.

5.2. Model calibration and discussion

Note that for the specific velocity profile, this model can change the angular velocity in two ways given below in equation 3.18 and 3.19.

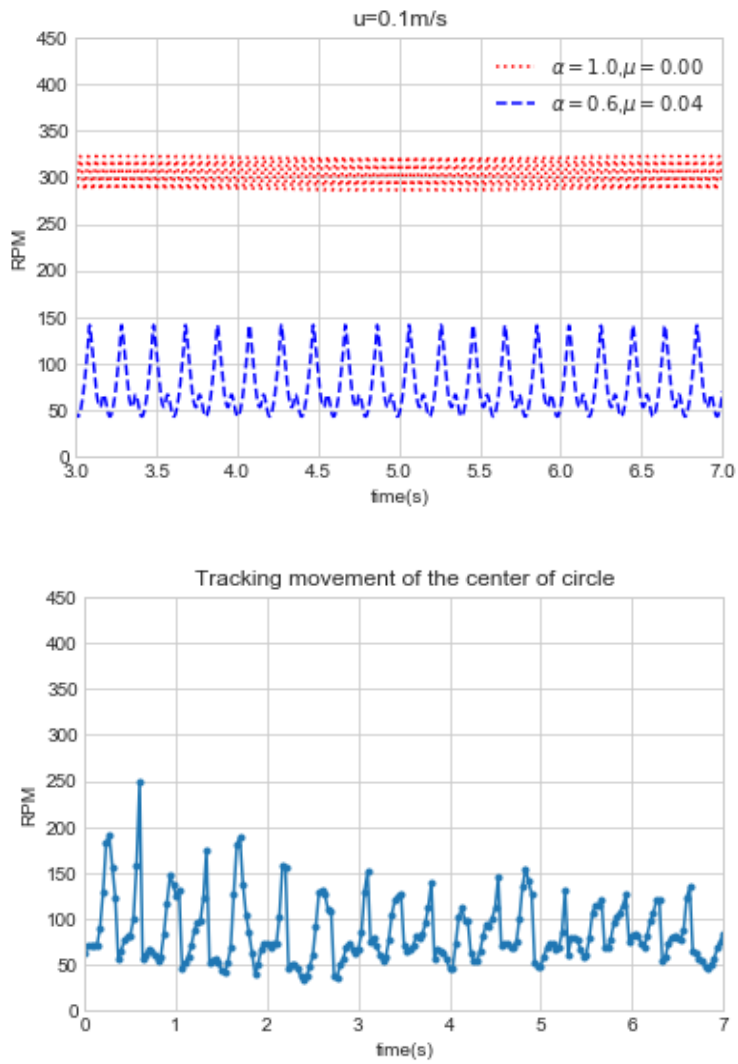

Fig. 40. Example of calibration by changing two coefficients; (upper) model, (lower) experiment

The process of calibrating model parameters is in Fig. 40. Starting from ideal case (dotted line), by changing the model parameters to match with the experimental results based on its mean and fluctuation values. Then, defining the adjustment parameters (velocity induction and friction) by using least square method. The results of adjusting numerical model by calibrated parameters are given in Fig. 41 with the experimental results.

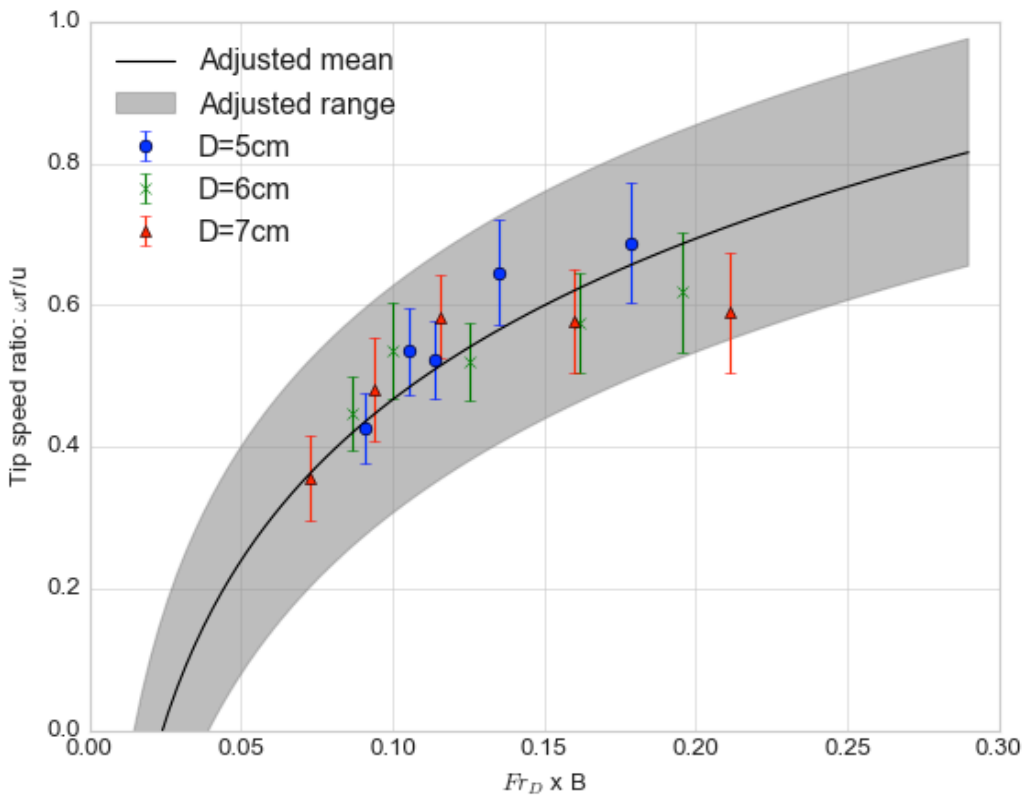

Fig. 41. Experimental results with adjusted model, $R^2 = 0.8340$

From numerous work, the empirical equation of velocity induction factor a is given as

$$a = 0.33\ln(\mathrm{Fr}_D\mathrm{B})+0.70 \tag{4.6}$$

The friction factor μ is

$$\mu = 0.05\ln(\mathrm{Fr}_D\mathrm{B})+0.01 \tag{4.7}$$

Note that the input variables are given as the product of Froude number and Blockage ratio. It leads that if we know the diameter and mean velocity of turbine at specific point, the tip speed ratio of turbine can be obtained from empirical relationship given by equation 5.2 and 5.3. Figure 38 shows the experimental results with adjusted model based on empirical equation. Adjusted mean is the mean tip speed ratio in equilibrium condition, while the adjusted range is containing the fluctuating ranges in given model.

To match with the experimental results, the mean and fluctuation values should be larger with the Froude number and Blockage ratio. Also, the mean values may have upper limit in given range. Note that it is almost impossible that the x-axis $\mathrm{Fr}_D\mathrm{B}$ has larger than 1. It is because if we have 10 m turbine, $\mathrm{Fr}_D\mathrm{B}$=1 requires h=10 m and u = 6 m/s which is not appropriate condition in given turbine device. Therefore, in given range, this empirical equation can be easily and appropriately applied in real situation.

The limitation of this model is that since it is simplified model, the other effects such as biological, turbulent flow, and arrangement issues between turbine are hard to discuss. However, the main advantage of this model is very cheap and considers the physical properties which is important to design the turbine device in estuary. The convergence time of this model is very quick that almost every condition, it converges to the equilibrium state within 1,000 steps with time step 0.01 s.

6. Conclusion

The main objectives of this study are constructing simplified numerical model for THAWT and calibrating the target adjustment parameters them with the experimental work. Due to the complexity of analysis for the cross-flow turbine, the BEMT based model is chose to apply the blade oriented force equilibrium equations based on the form of ordinary differential equations. Through this model, the angular velocity, torque, power coefficient and generated power can be determined in each numerical time step.

In numerical model, there are two adjustment model parameters. One is the velocity induction factor and the other is the friction coefficient. Without them, in ideal case, the model exaggerates the turbine model by making more than 5 times of energy rather than experimental works. With adjustment parameters, the time mean rotational speed of turbine can be deduced and the fluctuation of the RPM is also changed.

For experiment, the similitude and flow conditions are determined through the dimensional analysis and non-dimensional parameters. Then, the flow profile of flume is captured by Vectrino with error range. The small-scale turbines are made from 3D printer with 3 different sizes by self-assembly type turbine to deal with

the limit of 3D printing. The motion of turbine is measured by the image-processing by attaching the red and blue circle shape objects. The two objects can enhance the accuracy of capturing images and overcome the uncertainty from blurring effects.

The results from experiment are expressed as the relationship between the combination of three non-dimensional parameters; turbine Froude number, blockage ratio and tip speed ratio. As the product of turbine Froude number and blockage ratio is getting larger, the tip speed ratio tends to increase and converges to the limit. Based on the experimental results the constructed numerical model parameters are adjusted by matching the angular velocity of turbine. The mean and fluctuation of angular velocity are the target values to minimize the target function based on least square method. The empirical equation is derived and can be obtained from the geometry of turbine and flow conditions such as mean velocity and water depth. In application, it will be used to evaluate the energy potential of certain estuarine area where the water depth and velocity profile is specified.

References

[1] Adrian, R. J., & Westerweel, J. (2011). *Particle image velocimetry* (No. 30). Cambridge University Press.

[2] Anderson Jr, J. D. (2010). *Fundamentals of aerodynamics.* Tata McGraw-Hill Education.

[3] Antheaume, S., Maître, T. & Achard, J.-L. (2008). Hydraulic Darrieus turbines efficiency for free fluid flow conditions versus power farms conditions, Renewable Energy, 33, (10), pp. 2186-2198.

[4] Batten, W. M. J., Bahaj, A. S., Molland, A. F., & Chaplin, J. R. (2006). Hydrodynamics of marine current turbines. Renewable energy, 31(2), 249-256.

[5] Batten, W. M., Harrison, M. E., & Bahaj, A. S. (2013). Accuracy of the actuator disc-RANS approach for predicting the performance and wake of tidal turbines. Phil. Trans. R. Soc. A, 371(1985), 20120293.

[6] Betz, A. (1920). Das Maximum der theoretisch möglichen Ausnutzung des Windes durch Windmotoren. Zeitschrift fur das gesamte Turbinenwesten, 20.

[7] Bryden, I. G., Naik, S., Fraenkel, P., & Bullen, C. R. (1998). Matching tidal current plants to local flow conditions. Energy, 23(9), 699-709.

[8] Burton, T., Jenkins, N., Sharpe, D., & Bossanyi, E. (2011). *Wind energy handbook*. John Wiley & Sons.

[9] Carrigan, T. J., Dennis, B. H., Han, Z. X., & Wang, B. P. (2012). Aerodynamic shape optimization of a vertical-axis wind turbine using differential evolution. ISRN Renewable Energy, 2012.

[10] Darrieus, G. (1931). Turbine Having its Rotating Shaft Transverse to the Flow of Current. US Patent 1834018.

[11] Denny, E. (2009). The economics of tidal energy. Energy Policy, 37(5), 1914-1924.

[12] Draper, S. (2011). Tidal stream energy extraction in coastal basins. Univ. Oxford, DPhil Thesis, 253.

[13] Fujisawa, N., & Shibuya, S. (2001). Observations of dynamic stall on Darrieus wind turbine blades. Journal of Wind Engineering and Industrial Aerodynamics, 89(2), 201-214.

[14] Froude, R. E. (1889). On the part played in propulsion by differences of fluid pressure. Trans. Inst. Naval Architects, 30, 390.

[15] Houlsby, G. T., Draper, S., & Oldfield, M. L. G. (2008). Application of linear momentum actuator disc theory to open channel flow. Report no. OUEL, 2296(08).

[16] Khan, M. J., Bhuyan, G., Iqbal, M. T., & Quaicoe, J. E. (2009). Hydrokinetic energy conversion systems and assessment of horizontal and vertical axis turbines for river and tidal applications: A technology status review. Applied energy, 86(10), 1823-1835.

[17] Loth, J. L., & McCoy, H. (1983). Optimization of Darrieus turbines with an upwind and downwind momentum model. Journal of Energy, 7(4), 313-318.

[18] Leclerc, C., (1997). Why use natural laminar low airfoils in vertical axis wind turbine applications Aerospace Sciences 35th meeting and exhibit; Reno.

[19] Maître, T., Amet, E., & Pellone, C. (2013). Modeling of the flow in a Darrieus water turbine: Wall grid refinement analysis and comparison with experiments. Renewable Energy, 51, 497-512.

[20] Masson, C., Leclerc, C., & Paraschivoiu, I. (1998). Appropriate dynamic-stall models for performance predictions of VAWTs with NLF blades. International Journal of Rotating Machinery, 4(2), 129-139.

[21] McAdam, R. (2011). Studies into the technical feasibility of the Transverse Horizontal Axis Water Turbine (PhD thesis). Oxford University, UK.
Newman, B. G. (1984). Actuator-disc theory for vertical-axis wind turbines. In Wind Engineering 1983, Part 3C (pp. 347-355).

[22] Nortek, A. S. (2009). Vectrino velocimeter user guide. Nortek AS, Vangkroken, Norway, 621.

[23] Paraschivoiu, I. (2002). *Wind turbine design: with emphasis on Darrieus concept*. Presses inter Polytechnique.

[24] Paraschivoiu, I., & Delclaux, F. (1983). Double multiple streamtube model with recent improvements (for predicting aerodynamic loads and performance of Darrieus vertical axis wind turbines). Journal of energy, 7(3), 250-255.

[25] Rourke, F. O., Boyle, F., & Reynolds, A. (2010). Tidal energy update 2009. Applied Energy, 87(2), 398-409.

[26] Sheldahl, R. E., & Klimas, P. C. (1981). Aerodynamic characteristics of seven symmetrical airfoil sections through 180-degree angle of attack for use in aerodynamic analysis of vertical axis wind turbines (No. SAND-80-2114). Sandia National Labs., Albuquerque, NM (USA).

[27] Shiono, M., Suzuki, K., & Kiho, S. (2000). An experimental study of the characteristics of a Darrieus turbine for tidal power generation. Electrical Engineering in Japan, 132(3), 38-47.

[28] Solomon, S., Qin, D., Manning, M., Averyt, K., & Marquis, M. (Eds.). (2007). Climate change 2007-the physical science basis: Working group I contribution to the fourth assessment report of the IPCC (Vol. 4). Cambridge university press.

[29] Strickland, J. H. (1975). Darrieus turbine: a performance prediction model using multiple streamtubes (No. SAND-75-0431). Sandia Labs., Albuquerque, N. Mex. (USA).

[30] Templin, R. J. (1974). Aerodynamic performance theory for the NRC vertical-axis wind turbine. NASA STI/Recon Technical Report N, 76.

[31] Voulgaris, G., & Trowbridge, J. H. (1998). Evaluation of the acoustic Doppler velocimeter (ADV) for turbulence measurements. *journal of atmospheric and oceanic technology*, *15*(1), 272-289.

국문 초록

유속 분포를 고려한 Transverse Horizontal Axis Water Turbine 의 조류 에너지 추출 모델 개발

이창희

터빈의 효율을 평가하는 것은 재생 에너지의 경제성 및 엔지니어링의 적용에 있어 매우 중요하다. 이는 유체의 속도, 밀도, 터빈의 재료 및 기하학적 특성과 같은 다양한 요소에 영향을 받으며, 그동안 터빈을 흐름의 반대방향으로 일정한 추력을 작용하는 단일 디스크로 가정함으로써 단순화 하여 해석하는 LMADT (Linear Momentum Actuator Disc Theory)가 축류 터빈을 분석하기 위해 채택되었다.

한편 많은 조류 터빈들 중에서 옥스포드 대학에서 최근에 개발 된 Transverse Horizontal Axis Water Turbine (THAWT)은 조류 터빈으로 많은 이점을 가진 교차류 터빈이다. 이는 양방향 흐름에서 일정한 효율을 가지며 축 방향으로 쉽게 연장 될 수 있으며 구조적으로 안정하다. 그러나 교차류 터빈은 축류 터빈보다 복잡한 메커니즘을 가지고 있기 때문에 LMADT 를 THAWT 에 직접 적용하는 것은 어렵다. 또한, 교차류 터빈의 경우, 블레이드의 절반이 유동 방향과 반대 방향으로 회전하기 때문에 유속 분포의 존재가 터빈의 동력 계수에 영향을 미칠 것으로 보인다.

본 연구에서는 유속 분포를 갖는 THAWT 의 동력 계수를 얻기 위해 일반적인 LMADT 를 직접 적용하는 대신에 블레이드에 작용하는 물리적 특성을 분석하는 방법 인 블레이드 요소 모멘텀 이론(BEMT)을 적용한다. 이를 이용하는 것은 교차류 터빈을 분석 할 때 두 가지 이점이 있다. 하나는 LMADT 접근법의 한계를 극복하고 다른 하나는 BEMT 를 통해 양력 및 항력을 얻어 터빈에 직접 작용하는 힘을 고려하기 때문에 속도 프로파일을 고려할 수 있다는 것이다. 이를 기반으로 간단한 해석 형식을 통한 모델을 구성한 후 터빈의 출력 계수를 수치 적으로 얻는다. 이후 모델의 조정 계수로 LMADT 이론을 기반으로 도입한 속도 감소 계수 및 수직 항력과 마찰 요소를 고려한 마찰 계수를 두어 3D 프린터를 통해 제작한 모형 터빈 실험과 비교해 검증한다.

구축한 수치 모델 및 실험 결과를 통해 터빈의 끝단속도비에 영향을 주는 요소를 수심, 터빈의 지름, 상류의 시간 평균 유속 및 중력가속도를 바탕으로 한 무차원수들의 조합으로 나타내었다. 이 관계를 통해 속도 감소 계수 및 마찰 계수로 표현한 조정 계수를 경험식을 통해 나타낼 수 있고, 실험 결과와 비교하여 $R^2 = 0.8340$ 의 정확도를 보였다. 본 연구를 통해 수심 및 유속 정보를 얻을 수 있는 연안 지역에 최적 터빈 설치 위치 및 잠재량 등을 평가함에 있어 간단하고 빠른 결과를 제공할 수 있을 것이다.

주요어: 조류 에너지, THAWT, BEMT, 교차류 터빈

학번: 2017-29440